Techno-economic assessment of integrated spectral-beam-splitting photovoltaic-thermal (PV-T) and organic Rankine cycle (ORC) systems

Peacock, Joshua; Huang, Gan; Song, Jian; Markides, Christos N.

DOI:
10.1016/j.enconman.2022.116071

Document Version
Publisher's PDF, also known as Version of record

Citation for published version (Harvard):
Peacock, J, Huang, G, Song, J & Markides, CN 2022, 'Techno-economic assessment of integrated spectral-beam-splitting photovoltaic-thermal (PV-T) and organic Rankine cycle (ORC) systems', *Energy Conversion and Management*, vol. 269, 116071. https://doi.org/10.1016/j.enconman.2022.116071

Energy Conversion and Management 269 (2022) 116071

Contents lists available at ScienceDirect

Energy Conversion and Management

journal homepage: www.elsevier.com/locate/enconman

Techno-economic assessment of integrated spectral-beam-splitting photovoltaic-thermal (PV-T) and organic Rankine cycle (ORC) systems

Joshua Peacock, Gan Huang [*,1], Jian Song [1], Christos N. Markides

Clean Energy Processes (CEP) Laboratory, Department of Chemical Engineering, Imperial College London, London SW7 2AZ, UK

ARTICLE INFO

Keywords:
Cogeneration
Combined heat and power
Organic Rankine cycle
Photovoltaic-thermal
Renewable energy
Solar energy
Techno-economic

ABSTRACT

Promising solar-based combined heating and power (CHP) systems are attracting increasing attention thanks to the favourable characteristics and flexible operation. For the first time, this study explores the potential of integrating a novel spectral-beam-splitting (SBS), hybrid photovoltaic-thermal (PVT) collector and organic Rankine cycle (ORC) technologies to maximise solar energy utilisation for electricity generation, while also providing hot water/space heating to buildings. In the proposed collector design, a parabolic trough concentrator (PTC) directs light to a SBS filter. The filter reflects long wavelengths to an evacuated tube absorber (ETA), which is thermally decoupled from the cells in the PVT tube, subsequently enabling a high-temperature fluid stream to be provided by the ETA to an ORC sub-system for secondary power generation. The SBS filter's optical properties are a key determinant of the system's performance, with maximum electricity generation attained when the filter transmits wavelengths between 485 and 860 nm onto the PVT tube, while the light outside this range is reflected onto the ETA. The effect of key design parameters and system capacity on techno-economic performance is investigated, considering Spain (Sevilla), the UK (London) and Oman (Muscat) as locations to capture climate and economic impacts. When operated for maximum electricity generation, the combined system achieves a ratio of heat to power of ~1.3, which is comparable to conventional CHP systems. Of the total incident solar energy, 24% and 31% is respectively converted to useful electricity and heat, with 54% of the electricity being generated by the PV cells. In Spain, the UK and Oman, respective electricity generation of 1.8, 0.9 and 2.1 kWh_{el}/day per m^2 of PTC area is achieved. Energy prices are found to be pivotal for ensuring viable payback times, with attractive payback times as low as 4–5 years obtained in the case of Spain at system capacities over 2.7 kW_{el}. Integrating the ORC sub-system with the concentrating SBS-PVT collector design reduced the levelised cost of electricity ($LCOE_{el}$). A $LCOE_{el}$ of 0.10 £/kWh is attained in Spain at an electrical capacity of only 4 kW_{el}, demonstrating the significant potential of exploiting the proposed systems in practical applications, as highly competitive with established combustion-based CHP systems.

1. Introduction

Of total global primary energy consumption, approximately 30% is attributed to power and heat supply to residential and commercial buildings [1]. To decarbonise this energy supply, it is imperative that research efforts, such as those presented in this paper, are aimed at exploring and developing economically competitive technologies. Although barriers still exist, there are feasible pathways to decarbonise the power sector, with the share of global electricity generation from renewables increasing to approximately 30% in 2021 [2]. Decarbonising the heat provision to buildings, however, remains an open challenge, especially in countries where homes are still reliant on comparatively cheap gas supply.

Decarbonising the buildings sector will likely require several solutions in tandem, one of which is the use of combined heat and power (CHP) systems. CHP systems generate electricity while providing useful thermal energy and are scalable in suppling both electricity and heat to individual buildings, industrial processes or larger communities via district networks. Efficiency is also enhanced by locality, avoiding transmission and distribution losses. Overall efficiencies of up to 90% can be attained, with significantly higher fuel-energy savings ratios (FESRs) than conventional electricity generation and onsite boilers [3,4]. Conventional CHP systems are typically thermally-driven by fossil

* Corresponding author.
E-mail address: g.huang@imperial.ac.uk (G. Huang).
[1] The two authors have the same contribution to this study.

https://doi.org/10.1016/j.enconman.2022.116071
Received 20 May 2022; Received in revised form 23 July 2022; Accepted 27 July 2022
Available online 11 August 2022

Nomenclature

A	Area, m^2
A'	Solar cell ideality factor
b	Solar cell empirical parameter
c	specific heat capacity of Therminol VP-1, J/(kg•K)
c_w	specific heat capacity of water, J/(kg•K)
C_{capex}	Capital cost, £
$C_{O\&M}$	Operating and maintenance cost, £/yr
$D_{ut,i}$	Inner diameter of ETA U-tube, m
D	Discount rate
e	electron charge, C
E	Electrical energy output, W
E_{bg}	Bandgap energy, eV
FF	Fill factor
G	Solar irradiance, W/m^2
h	Heat transfer coefficient, $W/(m^2•K)$
h	Specific enthalpy, J/kg
IR	Inflation rate, %
$I_{AM1.5}$	Air mass 1.5 spectral irradiance, $W/(m^2•nm)$
J_{ds}	Dark saturation current, A
J_{sc}	Short circuit current, A
k	Thermal conductivity, W/(m•K)
k_B	Boltzmann constant, J/K
k_1	Solar cell empirical parameter
L	Length, m
$LCOE$	Levelised cost of energy, £/kWh
$LMTD$	Log mean temperature difference, K
m	Mass flow rate, kg/s
n	Lifetime, year
NS	Net savings, £/year
Nu	Nusselt number
P_{drop}	Pressure drop, Pa
PBT	Payback time, year
Pr	Prandtl number
PR	Energy price rate, £/kWh
Q	Thermal energy output, W
Re	Reynolds number
SR	Spectral response, A/W
St	Stanton number
T	Temperature, °C
u_{wind}	Wind velocity, m/s
U	Overall heat transfer coefficient, $W/(m^2•K)$
V	Volume, L
V_{oc}	Open circuit voltage, V
W	Width W
W	Work, W
z	Solar cell empirical parameter

Greek

α	Absorptivity
β	Solar cell temperature coefficient, %/K
γ	Shaded PTC region
ε	Emissivity
η	Efficiency, %
λ	Wavelength, nm
μ_b	Viscosity in bulk, Pa•s
μ_w	Viscosity at wall, Pa•s
ρ	Reflectivity
τ	Transmissivity

Subscripts

a	Ambient
abs	Absorbed
avg	Average
AM1.5	Air mass 1.5
cd	Conductive
cp	Circulation pump
ct	Copper tubing of ETA
cv	Convective
CT	Cold tank
el	Electrical/electricity
ent	Entrance
evap	Evaporator
exp	Expander
ETA	Evacuated tube absorber
F	SBS filter
g	PV cover glass
gen	Generator
HT	Hot tank
HTF	Heat transfer fluid
HX	Heat Exchanger
ig	Inner absorptive glass of ETA
og	Outer glass of ETA
ORC	Organic Rankine cycle
p	Pump
PTC	Parabolic trough concentrator
PV	Photovoltaic cell
PVT	Photovoltaic-thermal
r	Radiative
s	Solar or entropy
std	Standard conditions
t	Outer tube glass of PVT
th	Thermal
TES	Thermal energy storage
w	Water

fuels, and despite short-term efficiency benefits, this will not enable full decarbonisation. A flexible, scalable, and cost-competitive renewable-energy-driven CHP system would facilitate fast decarbonisation of the buildings sector. Solar-based CHP systems can generate both power and useful thermal energy for hot water, space heating and/or cooling. As this present research explores, various technologies can be incorporated to increase the overall efficiency of solar energy utilisation and reduce the costs of co-generation. This makes solar-CHP systems a highly promising and potentially cost-competitive option for decarbonising power and heat supply to buildings.

Solar-thermal collectors are wavelength-independent, capturing solar energy as heat to provide hot water or space heating. Photovoltaic (PV) panels are widely used at both grid and household scales, generating electricity in a quantum process from photons at or above the semiconductor band gap energy. PV cells are therefore highly responsive within a specific spectral window. Photons of wavelengths outside this window are converted to heat, subsequently raising the temperature and reducing the electrical efficiency of PV cells.

Hybrid photovoltaic-thermal (PVT) collectors integrate PV cells with thermal absorbers, enabling CHP generation from the same installed area, increasing practicality and reducing costs for building-integrated installations [5]. Flat-plate PVT collectors use a heat transfer fluid (HTF) to remove the heat generated in the PV cells, thereby improving their electrical efficiency. The overall efficiency of a PVT collector is usually higher than that of a separate solar-thermal collector or PV panel [6,7]. Numerous studies demonstrate the significant techno-economic potential of hybrid PVT-CHP systems to supply residential buildings [8–10], however, these systems are typically limited to low fluid

temperatures in order to maximise the PV efficiency. Higher performance at fluid outlet temperatures above 60 °C, as needed by domestic hot water provision and space heating, is required to become a more competitive solar converter [11]. To make these technologies more economically viable and increase their uptake, additional investment is required to reduce upfront costs and develop the infrastructure within which they operate [12–14]. The performance of PVT collectors can be improved by using an optical concentrating device to increase the incident solar intensity per unit area. The PV area required in a concentrated PVT (CPVT) CHP system is significantly reduced for the same output. This reduces the system cost, enabling the use of more expensive, efficiency-enhancing components such as III-V high-efficiency solar cells and solar-tracking concentration systems [14]. A higher HTF temperature of over 80 °C is also obtainable due to the increased solar intensity [14], widening the applicability to different end-users. However, the electrical efficiency of CPVT-based CHP systems is reduced at the high operating temperatures of the PV cells under high solar concentration ratios [15,16].

Spectral beam splitting (SBS) offers a solution to this problem, whereby an optical filter selectively splits the incident solar spectrum into two discrete wavelength bands to be used separately, thermally decoupling the electrical and thermal system components [17,18]. Through this method, the wavelengths directed onto the PV cells can be optimised to reduce the generation of waste heat. The remaining spectrum is absorbed by a separate solar-thermal receiver, enabling higher temperatures to be obtained, which is better suited to CHP applications, without overheating PV cells [18]. Various SBS concepts have been studied and prototyped for use in PVT systems, with the use of different materials, configurations and modelling techniques being explored.

Selectively absorptive fluid filters are one approach, acting both as a thermal receiver and spectral filter. In recent years, numerous studies have used numerical simulations and experimental prototypes to explore the ability of different nanoparticles to promote better spectral matching and, thus, to achieve greater efficiency gains with promising results [19–24]. Multi-layer, thin-film interference filters are a common spectral-splitting design that use various materials to achieve better tuning to match the spectral response of PV cells and have been shown to benefit the performance of PVT-CHP systems significantly. Some of the most notable recent studies include the experimental investigation by Liang and Wang et al. [25], who studied the use of a SiO_2/TiO_2 interference thin film which increased PV efficiency by up to 10% and resulted in an overall PVT energy efficiency close to 23%. A further relevant study by Wang et al. [26] considered employing this optical filter type in a SBS-CPVT system for a dairy farm and the results showed that the SBS-CPVT solar system was economically viable if the cost of the optical filter was <75% of that of the parabolic trough solar concentrator. Huang et al. [27] provided widely applicable research studying optimal SBS filter limits to maximise the performance of PVT collectors when using a range of PV materials, including Si and GaAs. A real SBS-CPVT system was fabricated and tested by Wingert et al. [28] based on a commercial parabolic trough solar concentrator. A 1.7-m-long large-scale dichroic mirror was used to separate spectrally the solar spectrum. Their outdoor tests demonstrated that the SBS-CPVT system was able to improve the power output by ~13% relative to an existing parabolic trough powerplant. In another recent study by Liew et al. [29], both the solar cells and optical filter (a commercially-available product from company 3M) were coated onto the reflector surface of a parabolic trough solar concentrator. Their simulation results showed that the annual power output of the SBS-CPVT system was ~9% higher than that of a running solar electric generating station VI parabolic trough plant in California. Another interesting approach has been proposed using semi-transparent PV cells, such as CdTe, perovskite and polymer cells, to perform the spectral-splitting function, removing the need for additional optical components [30]. It is clear from the literature that SBS-based PVT systems, if appropriately designed, have the potential to enable better overall solar utilisation than conventional PVT systems.

Solar-powered organic Rankine cycle (ORC) systems are an alternative, non-PV approach to achieving power [31] and CHP generation [32]. The ability of solar-ORC systems with thermal energy storage (TES) to meet variable domestic heat and power demand is well demonstrated by some notable studies[32–34]. Research on CHP systems combining a PVT collector with an ORC sub-system in order to improve electrical performance is limited, however certain configurations have shown great potential for specific applications. In 2016, Al-Nimr et al. [35] investigated a CPVT-ORC CHP system integrating geothermal cooling and an energy storage unit, and found that the electrical efficiency of this system was improved by 16–18% due to the integration of the ORC sub-system. Wang et al. [36] also demonstrated the promise of a PVT-ORC system in a real-life application of CHP provision to swimming pools, with the ORC sub-system improving the system's ability to meet the local energy demands with a desirable payback time of 12.7 years. The advantage of PVT-ORC systems in meeting variable domestic electricity demands was further demonstrated by Kutlu et al. [37], who showed that the highest daily power output was twice that of standalone solar-ORC systems, and 24% higher than that of standalone PV systems. While integrated PVT-ORC CHP systems show promise, economic performance is still limited by the reduced PV efficiency and lower fluid temperatures attained in comparison to thermally decoupled SBS-based systems, such as that proposed in this paper.

In this study, we integrate for the first time a SBS-CPVT solar collector with an ORC sub-system, in order to explore the potential and performance of such a hybrid solar system, which can be a promising option for CHP applications. This is because, as well as improving PVT co-generation efficiency through spectral splitting, high-temperature HTFs can be obtained, decoupled from the PVT tube, subsequently allowing a higher efficiency of the ORC sub-system. Maximising co-generation through this integration enables an economically competitive solar-CHP system. This study presents a techno-economic analysis of a SBS-CPVT-ORC (integrated SBS-CPVT and ORC sub-system) system for CHP provision in the domestic sector. A whole-system physical model is developed to simulate the techno-economic performance, and parametric analyses are performed to obtain insight into the system's operation. A range of regions, including Spain, the UK and Oman, are selected for performance evaluation to assess the influence of regional climate conditions and economic parameters on the proposed system. Finally, the system cost is benchmarked against existing/conventional CHP technologies to address the potential for practical applications.

2. System description

Fig. 1 shows a schematic of the proposed system. The main components include a SBS-CPVT collector employing a PTC, two fluid-storage tanks, two heat exchangers for domestic heating purposes and an ORC sub-system for secondary power generation from the hot fluid delivered by an ETA.

The solar spectrum is reflected by a PTC onto the SBS filter. The SBS filter transmits a portion of the spectrum onto the evacuated PVT tube, where the PV cells generate electricity. A HTF is circulated through the PVT tube, generating low-grade excess heat (<100 °C), which is subsequently used to heat the water in Heat Exchanger 1 (HX1).

The SBS filter reflects the remaining portion of the solar spectrum onto the evacuated tube absorber (ETA), where the circulating HTF captures the high-temperature heat. *Therminol VP-1* is used as the HTF within both the PVT tube and ETA loop thanks to its thermal stability and uniform performance within a wide range of temperatures (12–400 °C) [38]. This high-temperature fluid from the ETA is held up within the thermally-insulated TES hot tank, acting as a storage medium. The flow rate of the HTF from the hot tank to the ORC evaporator is constant, ensuring consistent loading and electricity generation. Excess thermal energy unused by the ORC sub-system is then utilised to heat the water in Heat Exchanger 2 (HX2), before being stored at

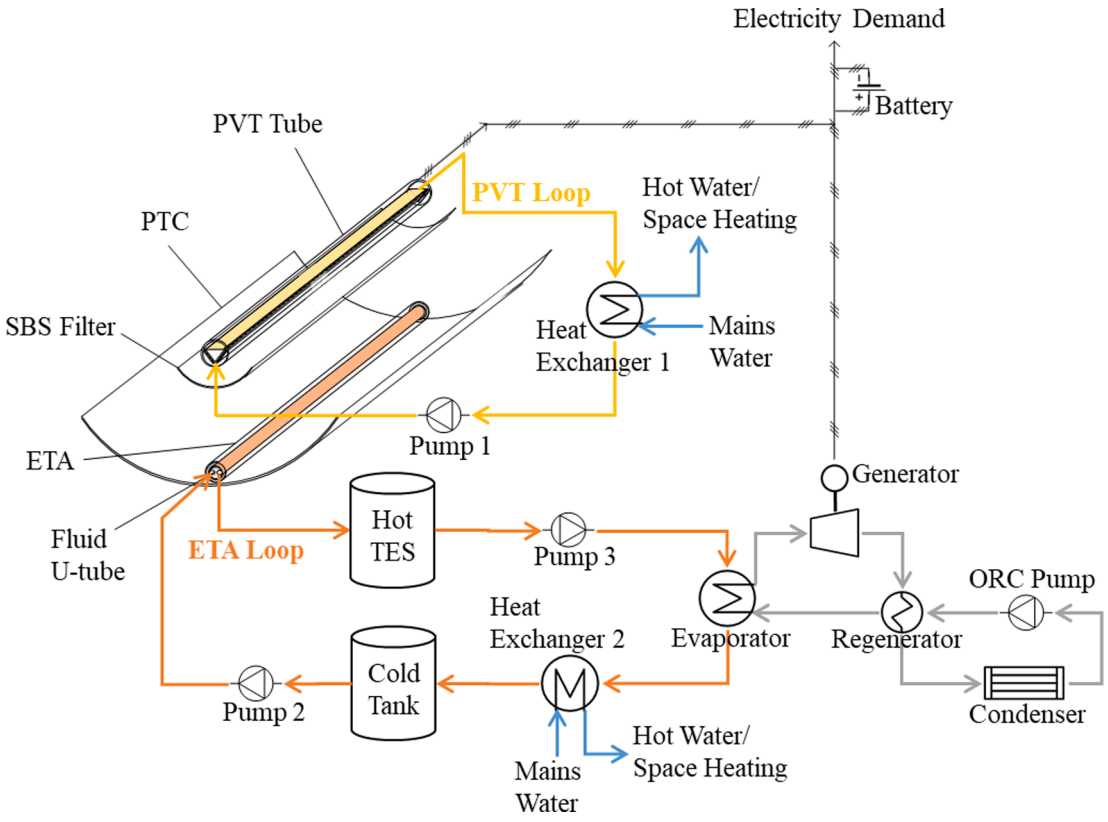

Fig. 1. Schematic of an integrated SBS-CPVT-ORC system for solar heat and power provision.

ambient conditions in the cold storage tank. A battery is also included in the system to balance the electricity generation and domestic demand.

2.1. SBS-CPVT collector design

A simplified cross-sectional diagram of the collector is shown in Fig. 2(a). A tracked PTC is used as it is suited to a SBS system [14], while offering a good balance of cost, stability and high optical efficiency, with a reflectivity over 0.95 being achievable using a variety of materials [39]. A dichroic interference selectively-reflective SBS filter is considered as it can be manufactured to achieve specific long pass, short pass and multi-band cut-off wavelengths [40]. The filter area is set to 20% of the concentrator [18].

As shown in Fig. 2b, an evacuated glass tube encases the PVT part to reduce the convective loss. The PVT is configured in a V-trough configuration to benefit thermal performance by increasing heat transfer into the fluid [41]. To reduce the radiative loss, the emissivity can be reduced from 0.9 to ~0.15 [11] by applying coatings to the PV cover glass, often at a cost to transmissivity and hence the PV electrical efficiency. A high-performance silver-based coating is employed in the model ($\varepsilon = 0.13$, $\tau = 0.87$) [42], which can improve the thermal efficiency by a further 15% at a cost of only <1% electrical efficiency. Gallium Arsenide (GaAs) is considered as the PV material in this study, to attain high efficiencies under higher temperatures, due to a low efficiency-temperature loss coefficient of 0.08%/°C, compared to 0.41%/°C and 0.21%/°C for c-Si and CdTe cells, respectively [18].

The dimensions of the PTC, SBS filter and PVT tube are listed in Table 1, with a geometric concentration ratio of 10 and a PVT aperture area of 0.45 m^2. For simplification, a one-dimensional (1-D) numerical model is used to model the collector.

The ETA design is based on the configuration investigated by Ma et al. [43], with a vacuum between outer and inner glass tubes that are fused at one end. A coating ($\alpha = 0.92$, $\varepsilon = 0.08$) is applied to the surface of the inner glass layer to reduce radiative losses. The ETA dimensions

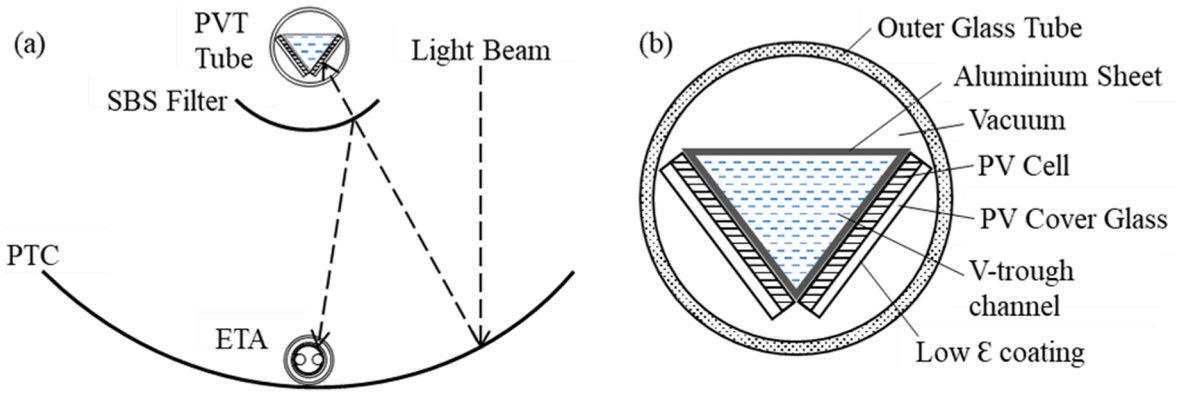

Fig. 2. Cross-sectional diagram of: (a) the overall SBS-CPVT collector, and (b) the PVT tube.

Table 1
Dimensions of PTC, SBS filter and PVT tube considered in this work.

Component	Width (m)	Length (m)	Area (m^2)	Thickness (m)
PTC	1.5	3	4.5	–
SBS filter	0.3	3	0.9	–
PVT outer glass tube	0.15	3	0.45	–
PV cover glass	0.15	3	0.45	0.04
PV cells	0.15	3	0.45	–
Fluid channel	0.15	3	0.45	0.01

are shown in Table 2, with only the length adjusted to match that of the collector.

The optical properties of each collector component are given in Table 3. The resulting individual optical efficiencies of the PVT tube and the ETA are 0.77 and 0.87, respectively, as a product of the outer layer(s) transmissivity and inner layer absorptivity. Incorporating overall system losses, including the shaded region on the parabolic mirror (using an intercept factor $\gamma = 0.93$) and the mirror reflectivity, optical efficiencies are reduced to 0.68 and 0.77, for the PVT tube and the ETA.

2.2. ORC sub-system

A regenerative ORC sub-system is selected to integrate with the SBS-CPVT collectors. The organic working fluid in the ORC sub-system is firstly pressurised by the pump and then heated in the regenerator. It then absorbs heat from the high-temperature ETA fluid in the evaporator and becomes saturated or superheated vapour. The organic vapour expands in the expander to generate power and is then cooled in the regenerator and condensed to a liquid state in the condenser before entering the pump again for the next cycle. Several organic working fluid candidates are considered [43–45], suitable for a range of operating temperatures, as shown in Table 4.

3. Modelling methodology

3.1. Solution method and regional characteristics

A numerical model of the proposed SBS-CPVT-ORC CHP system has been developed. The model captures optical and heat transfer mechanisms in the solar collector, determining energy available for electricity generation in the PV cells and ORC sub-system, and excess heat available for thermal-energy generation. The collector optical and thermal models and PV electrical model, employ the same approach and equations that have been extensively utilised and validated in previous literature on PVT-based systems [8,26,46]. Location-specific weather data and economic parameters are the input of the model, enabling computation of techno-economic parameters such as the total CHP output, efficiency, payback time (*PBT*), levelised cost of energy (*LCOE*) and demand cover.

The model is quasi-static, assuming steady-state solar irradiance for each hour. The 24-hour input solar profiles representing the average irradiance in a year for the considered locations are shown in Fig. 3. These profiles are formed using the global irradiance data from the European commission's PV geographical information system [48], with a two-axis tracking plane. Techno-economic assessments are conducted for Spain, as a European country with comparatively high solar irradiance and a significant renewables market, and also for the UK and Oman for comparative purposes. Key location-specific information is shown in Table 5.

Table 2
ETA dimensions for a small-scale domestic system [39].

Component	Thickness (m)	Length (m)	Inner diameter (m)	Outer diameter (m)	Outer area (m^2)
Outer glass tube	0.0012	3.0	–	0.047	0.44
Vacuum	0.0038	–	–	–	–
Inner glass absorber tube	0.0012	3.0	–	0.037	0.35
Copper fin	0.0006	3.0	–	0.033	0.31
Copper U-tube	0.0006	6.0	0.0068	0.008	0.15

Table 3
Optical properties of solar collector components.

Component	ε	τ	α	ρ	Ref.
PTC	–	0.00	0.05	0.95	[14]
PVT					[18]
Outer glass tube	0.90	0.95	0.01	0.04	
PV cover glass w/coating	0.13	0.87	0.08	0.05	
GaAs PV cell	-	0.00	0.93	0.07	
ETA					[43]
Outer glass	0.90	0.95	0.01	0.04	
Inner glass w/coating	0.08	0.00	0.92	0.08	

Table 4
Working fluid candidates for the ORC sub-system.

	Critical pressure, P_{crit} (bar)	Critical temperature, T_{crit} (°C)	Molecular mass (kg/kmol)
R245fa	36.1	153	134.1
Pentane	33.6	196	72.2
Hexane	30.6	235	86.2
Heptane	27.3	267	100.2
Benzene	48.8	298	78.1
Toluene	41.3	319	92.1

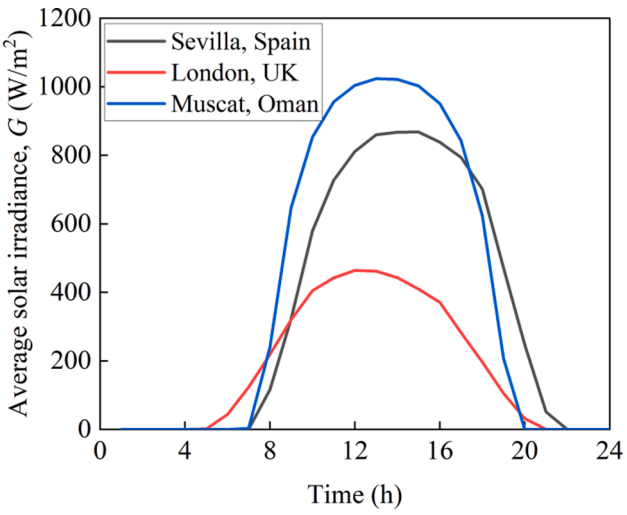

Fig. 3. Solar irradiance in the considered regions, taken as an average of all days in a typical year.

Table 5
Key location-specific information of the studied regions.

Country	Average ambient temperature, T_a (°C)	Electricity price, PR_{el} (£/kWh)	Gas price, PR_{gas} (kWh)	Household electricity demand (kWh_{el}/day)
Spain	18.6 [49]	0.20 [50]	0.08 [50]	10.4 [51]
UK	14.3 [52]	0.14 [53]	0.04 [53]	10.6 [54]
Oman	28.2 [55]	0.02 [56]	–	54.8 [57]

3.2. Collector optical model

The absorbable solar irradiance incident onto each component in the SBS-CPVT collector are calculated based on the optical properties listed in Table 3, forming inputs to the collector thermal model and PV electrical model.

A 1-D numerical model is used to calculate the optical performance of the collector. The solar irradiance incident on the PTC is determined relative to the reference AM1.5 spectral distribution, $I_{AM1.5}$. Fig. 4 shows $I_{AM1.5}$ and the SBS filter's cut-off wavelengths, λ_{min} and λ_{max}, relative to the GaAs-cell spectral response (*SR*). The SBS filter is modelled as ideal to explore the maximum potential of the system, where filter transmissivity, $\tau_F(\lambda)$, is equal to 1 between the cut-off wavelengths, and reflectivity, $\rho_F(\lambda)$, is equal to 1 outside these wavelengths.

The AM1.5 spectral irradiance, $I_{AM1.5}(\lambda)$, is integrated with respect to wavelength, λ, to calculate the reference solar irradiance, $G_{AM1.5}$,

$$G_{AM1.5} = \int_{280}^{4000} I_{AM1.5}(\lambda)\mathrm{d}\lambda. \tag{1}$$

Solar irradiance incident on the PVT tube G_{PVT} is calculated by integrating the reference spectral irradiance, $I_{AM1.5}(\lambda)$, and SBS filter transmissivity, $\tau_F(\lambda)$, over the spectrum. Irradiance energy density is also corrected by the ratio of the hourly average solar irradiance to the reference solar irradiance, $G/G_{AM1.5}$, as well as the geometric concentration ratio, A_{PTC}/A_{PVT},

$$G_{PVT} = \frac{G}{G_{AM1.5}}\gamma\rho_{PTC}\frac{A_{PTC}}{A_{PVT}}\int_{280}^{4000}\tau_F(\lambda)I_{AM1.5}(\lambda)\mathrm{d}\lambda, \tag{2}$$

where optical losses in the PTC are incorporated as a product of the shaded portion of the concentrator, γ, and the reflectivity, ρ_{PTC}. Solar irradiance incident on the ETA, G_{ETA}, is calculated by integrating the reference spectral irradiance, $I_{AM1.5}(\lambda)$, and filter reflectivity, $\rho_F(\lambda)$,

$$G_{ETA} = \frac{G}{G_{AM1.5}}\gamma\rho_{PTC}\frac{A_{PTC}}{A_{og}}\int_{280}^{4000}\rho_F(\lambda)I_{AM1.5}(\lambda)\mathrm{d}\lambda, \tag{3}$$

where A_{PTC}/A_{og} is the geometric concentration ratio between the PTC and outer glass area of the ETA.

The solar irradiance absorbed by the outer glass of the PVT tube, $G_{t,abs}$, is calculated by multiplying the tube absorptivity, α_t, by the sum of the irradiance incident on the outer surface and the irradiance reflected from the PV cover glass below,

$$G_{t,abs} = \alpha_t G_{PVT} + \tau_t\rho_g\alpha_t G_{PVT}, \tag{4}$$

where τ_t and ρ_g are the transmissivity of the outer glass tube and the reflectivity of the PV cover glass, respectively. Solar irradiance absorbed by the PV cover glass, $G_{g,abs}$, is similarly calculated, considering irradiance transmitted by the outer glass tube and reflected by the PV cells,

$$G_{g,abs} = \tau_t\alpha_g G_{PVT} + \tau_t\tau_g\rho_{PV}\alpha_g G_{PVT}, \tag{5}$$

where τ_g and α_g are the transmissivity and absorptivity of the PV cover glass, and ρ_{PV} is the reflectivity of the PV cells. Total solar irradiance absorbed by the PV cells, G_{PV}, is expressed as a product of the cell's absorptivity, α_{PV}, and the irradiance transmitted by the cover glass,

$$G_{PV} = \tau_t\tau_g\alpha_{PV}G_{PVT}. \tag{6}$$

The solar irradiance absorbed by the outer glass of the ETA, $G_{og,abs}$, is calculated from,

$$G_{og,abs} = \alpha_{og}G_{ETA} + \tau_{og}\rho_{ig}\alpha_{og}G_{ETA}, \tag{7}$$

where τ_{og} and α_{og} is the transmissivity and absorptivity of the ETA outer glass, and ρ_{ig} is the reflectivity of the inner glass. The inner glass is opaque due to the selective absorptive coating; thus the absorbed irradiance is composed only of the irradiance transmitted by the outer glass,

$$G_{ig,abs} = \tau_{og}\alpha_{ig}\frac{A_{og}}{A_{ig}}G_{ETA}, \tag{8}$$

where α_{ig} is the inner glass absorptivity, and A_{og}/A_{ig} is the geometric concentration ratio between the outer and inner glass.

3.3. PV electrical model

This section of the model aims to compute the PV cell electricity generation, E_{PV}, the cell's electrical efficiency, $\eta_{el,PV}$, and the portion of incident solar irradiance converted to heat in the cell, $G_{PV,abs}$. Table 6

Table 6
GaAs solar cell model parameters.

Parameter	Value	Ref.
Temperature coefficient (β)	0.08	[18]
Bandgap energy (E_{bg})	1.43	[59]
Ideality factor (A')	1	
Empirical parameter (k_1)	0.03	
Empirical parameter (b)	1.2	
Empirical parameter (z)	0.98	

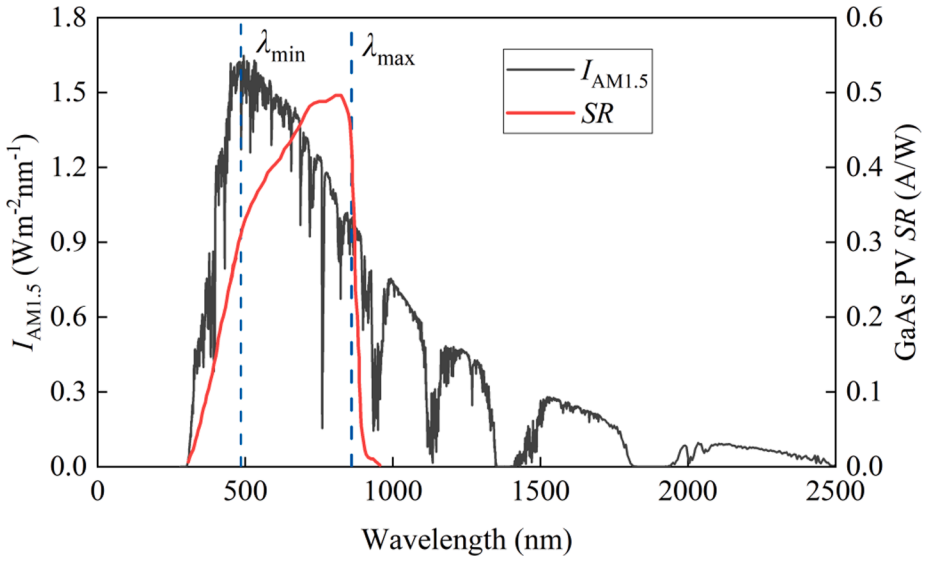

Fig. 4. AM1.5 spectral irradiance, modelled GaAs PV cell spectral response [58] and SBS transmissive bounds.

lists the input parameters for the PV model.

The dark saturation current, J_{ds}, is calculated from [60],

$$J_{ds} = k_1 T_{std}^{3/z} \exp\left(\frac{-E_{bg}}{bk_B T_{std}}\right), \tag{9}$$

where k_1, b and z are empirical parameters, E_{bg} the PV cell band gap energy, k_B the Stefan-Boltzmann constant, and T_{std} the standard temperature (25 °C). The short-circuit current, J_{sc}, is calculated by integrating over the spectral response of PV cells, $SR(\lambda)$ (shown in Fig. 4), and considering PVT optical losses [61],

$$J_{sc} = \frac{G}{G_{AM1.5}} \gamma \rho_{PTC} \frac{A_{PTC}}{A_{PVT}} \tau_t \tau_g \alpha_{PV} A_{PVT} \int_{280}^{4000} \tau_F(\lambda) I_{AM1.5}(\lambda) SR(\lambda) d\lambda. \tag{10}$$

The open-circuit voltage, V_{oc}, is calculated from [25,26],

$$V_{oc} = \frac{A' k_B T_{std}}{e} \ln\left(\frac{J_{sc}}{J_{ds}} + 1\right), \tag{11}$$

where A' is the PV cell ideality factor and e is the charge of an electron. The PV electrical efficiency is defined as the ratio of PV electricity generation at standard conditions to the solar energy incident onto the PVT tube, adjusted for the loss in efficiency at temperatures above standard conditions [61],

$$\eta_{el,PV} = \frac{V_{oc} J_{sc} FF}{A_{PVT} G_{PVT}} (1 - \beta(T_{PV} - T_{std})), \tag{12}$$

where FF is the filling factor [62] and T_{PV} and β are the PV cell temperature (determined in the thermal model) and temperature coefficient, respectively. The portion of absorbed solar irradiance not utilised by the PV cell, $G_{PV,abs}$, can then be calculated from,

$$G_{PV,abs} = G_{PV} - \eta_{el,PV} G_{PVT}. \tag{13}$$

3.4. Collector thermal modelling

Energy balances are constructed with respect to each element of the PVT tube and ETA, and solved iteratively in MATLAB to determine the temperature of each element. For both the ETA and PVT tubes, convective and conductive heat transfer in the evacuated space is assumed negligible.

3.4.1. PVT tube

The energy inputs for the outer glass tube are the absorbed solar irradiance, $Q_{s,t}$, and radiative heat from the PV cover glass, $Q_{r,g-t}$. Energy outputs include radiative and convective heat losses to the environment, $Q_{r,t-sky}$ and $Q_{cv,t-a}$, respectively. The energy balance is expressed as,

$$Q_{s,t} + Q_{r,g-t} = Q_{r,t-sky} + Q_{cv,t-a}, \tag{14}$$

corresponding to,

$$A_{PVT} G_{t,abs} + A_{PVT} h_{r,g-t}(T_g - T_t) = A_{PVT} h_{r,t-sky}(T_t - T_{sky}) + A_{PVT} h_{wind}(T_t - T_a), \tag{15}$$

where $h_{r,g-t}$, $h_{r,t-sky}$ and h_{wind} are the heat transfer coefficients for the corresponding heat vectors $Q_{r,g-t}$, $Q_{r,t-sky}$ and $Q_{cv,t-a}$, and T_t, T_g and T_a are the outer glass tube, the PV cover glass and ambient temperatures, respectively. The theoretical sky temperature, T_{sky}, is defined to determine radiative loss, and is expressed as $T_{sky} = 0.0552 T_a^{1.5}$ [63].

The energy balance of the cover glass on the PV cells is comprised of absorbed solar energy, $Q_{s,g}$, radiative loss to the outer glass tube, $Q_{r,g-t}$, and conductive loss to the PV cell, $Q_{cd,g-PV}$,

$$Q_{s,g} = Q_{r,g-t} + Q_{cd,g-PV}, \tag{16}$$

corresponding to,

$$A_{PVT} G_{g,abs} = A_{PVT} h_{r,g-t}(T_g - T_t) + A_{PVT} h_{cd,g-PV}(T_g - T_{PV}), \tag{17}$$

where $h_{cd,g-PV}$ is the conductive heat transfer coefficient between the cover glass and PV cells, and T_{PV} is the temperature of the PV cell.

The PV energy balance considers the solar irradiance absorbed as heat, $Q_{s,PV}$, conductive heat loss to the cover glass, $Q_{cd,g-PV}$, and convective heat loss to the HTF flowing over the cells,

$$Q_{s,PV} + Q_{cd,g-PV} = Q_{cv,PV-HTF}, \tag{18}$$

corresponding to,

$$A_{PVT} G_{PV,abs} + A_{PVT} h_{cd,g-PV}(T_g - T_{PV}) = A_{PVT} h_{cv,PV-HTF}(T_{PV} - T_{avg,PVT}), \tag{19}$$

where $h_{cv,PV-HTF}$ is the convective heat transfer coefficient between the PV cells and HTF, and $T_{avg,PVT}$ is the average temperature of the HTF inlet, $T_{in,PVT}$, and outlet temperatures, $T_{out,PVT}$.

The HTF balance simply equates the incoming convective heat, $Q_{cv,PV-HTF}$, to the heat flowing out of the system, $Q_{out,PVT}$, assuming the top of the fluid channel is well insulated and further energy loss from the fluid is negligible,

$$Q_{cv,PV-HTF} = Q_{out,PVT}, \tag{20}$$

corresponding to,

$$A_{PVT} h_{cv,PV-HTF}(T_{PV} - T_{avg,PVT}) = m_{PVT} c(T_{out,PVT} - T_{in,PVT}), \tag{21}$$

where m_{PVT} is the HTF mass flow rate. For the PVT model, the mass flow rate is specified as a parameter, thus outlet HTF temperature, $T_{out,PVT}$, varies as a function of solar intensity, G. The specific heat capacity of the fluid, c, is interpolated for the correct temperature from manufacturer data [64].

3.4.2. Evacuated tube absorber

The ETA thermal model is constructed similarly to the PVT model, however considering the variation in surface area for each element. The outer glass layer energy balance includes the absorbed solar irradiance, $Q_{s,og}$, the radiative heat from the inner glass, $Q_{r,ig-og}$, and the radiative, $Q_{r,og-sky}$, and convective, $Q_{cv,og-a}$, heat losses to the environment,

$$Q_{s,og} + Q_{r,ig-og} = Q_{r,og-sky} + Q_{cv,og-a}, \tag{22}$$

corresponding to,

$$A_{og} G_{og,abs} + A_{avg,og} h_{r,ig-og}(T_{ig} - T_{og}) = A_{og} h_{r,og-sky}(T_{og} - T_{sky}) + A_{og} h_{wind}(T_{og} - T_a), \tag{23}$$

where A_{og} is the outer surface area, $A_{avg,og}$ is average of the outer glass surface areas, T_{og} and T_{ig} are the outer and inner glass layer temperatures, and $h_{r,ig-og}$ and $h_{r,og-sky}$ are the heat transfer coefficients relevant to the radiation between the inner and outer glass and the radiative loss to the environment.

The ETA inner glass absorbs solar irradiance transmitted by the outer glass, $Q_{s,ig}$, loses heat radiatively to the outer glass, $Q_{r,ig-og}$, and conductively to the copper tubing, $Q_{cd,ig-ct}$,

$$Q_{s,ig} = Q_{r,ig-og} + Q_{cd,ig-ct}, \tag{24}$$

corresponding to,

$$A_{ig} G_{i,abs} = A_{avg,g} h_{r,ig-og}(T_{ig} - T_{og}) + A_{ct} h_{cd,ig-ct}(T_{ig} - T_{ct}), \tag{25}$$

where A_{ig} and A_{ct} are the inner glass and copper tubing surface areas, respectively, and $h_{cd,ig-ct}$ is the conductive heat transfer coefficient between the inner glass and the copper. The copper tubing temperature, T_{ct}, is assumed to be equal to the adjacent copper U-tube temperature.

The copper tubing heat balance simply equates the energy conduced from the inner absorptive glass, $Q_{cd,ig-ct}$, and the convective loss from the HTF flowing through the U-tube, $Q_{cv,ct-HTF}$,

$$Q_{cd,ig-ct} = Q_{cv,ct-HTF}, \tag{26}$$

corresponding to,

$$A_{ct}h_{cd,ig-ct}\left(T_{ig}-T_{ct}\right)=A_{ut}h_{cv,ct-HTF}\left(T_{ct}-T_{avg,ETA}\right), \quad (27)$$

where A_{ut} is the surface area of the copper U-tube containing the HTF, $h_{cv,ct-HTF}$ represents convective heat loss coefficient to the HTF, and $T_{avg,ETA}$ is the average temperature of the HTF inlet, $T_{in,ETA}$, and outlet temperatures, $T_{out,ETA}$.

The HTF balance equates the convective heat from the U-tube, $Q_{cv,ct-HTF}$, to the heat leaving the ETA system, $Q_{out,ETA}$,

$$Q_{cv,ct-HTF}=Q_{out,ETA}, \quad (28)$$

corresponding to,

$$A_{ut}h_{cv,ct-HTF}\left(T_{ct}-T_{avg,ETA}\right)=m_{ETA}c\left(T_{out,ETA}-T_{in,ETA}\right), \quad (29)$$

where m_{ETA} is the HTF mass flow rate. The ETA model equations are iteratively solved for the required m_{ETA}. The mass flow rate in the ETA varies as an inverse function of solar intensity, to maintain the set point temperature. The set point temperature is specified to maximise the power generated by the ORC sub-system.

3.4.3. Heat transfer coefficients

The radiative heat loss coefficient from component 'i' to the environment is calculated from [65],

$$h_{r,i-sky}=\varepsilon_i k_B\left(T_i^2+T_{sky}^2\right)\left(T_i+T_{sky}\right), \quad \text{for } i=\text{g, og} \quad (30)$$

where ε_i is the component emissivity. The radiative heat transfer coefficient between two layers in the PVT tube and ETA is calculated from [65],

$$h_{r,1-2}=\frac{k_B\left(T_1^2+T_2^2\right)(T_1+T_2)}{\frac{1}{\varepsilon_1}+\frac{1}{\varepsilon_2}-1}. \quad (31)$$

The conductive heat transfer coefficient through 'n' adjacent layers is calculated from,

$$h_{cd,1-2}=\frac{1}{\frac{W_1}{k_1}+\frac{W_2}{k_2}+\cdots+\frac{W_n}{k_n}}, \quad (32)$$

where W and k are the thickness and thermal conductivity of the respective layer. Assuming a wind velocity, u_{wind}, of 1 m/s, the PVT and ETA outer layer convective heat loss coefficient, h_{wind}, is expressed as [8],

$$h_{wind}=4.5+2.9\,u_{wind}.$$

Correlations from Hines and Maddox [66] are used to calculate the heat transfer coefficient for convection between the PV cell and HTF, $h_{cv,PV-HTF}$, assuming laminar flow between two plates,

$$h_{cv,PV-HTF}=\begin{cases}h_{ent}\frac{L_{ent}}{L}+\frac{7.54k_{HTF}}{2W_{gap}}\frac{L-L_{ent}}{L} & \text{if } L<L_{ent}\\ h_{ent} & \text{otherwise}\end{cases}, \quad (34)$$

where the hydraulic diameter is equivalent to two times the fluid channel depth, W_{gap}, and L is the total channel length. The length L_{ent} and thermal entrance region heat transfer coefficient h_{ent} are calculated from,

$$L_{ent}=0.05RePr\left(2W_{gap}\right), \quad (35)$$

$$h_{ent}=\frac{7.54+0.03\left(\frac{2W_{gap}RePr}{L_{ent}}\right)k_{HTF}}{1+0.016\left(\frac{2W_{gap}RePr}{L_{ent}}\right)^{\frac{2}{3}}2W_{gap}}. \quad (36)$$

The heat transfer coefficient for convection from the ETA U-tube to the HTF is calculated based on Sieder and Tate's correlations [67], where the approach depends on the flow regime. The Nusselt number used for laminar flow regimes ($Re<3000$), while the Stanton number otherwise used,

$$Nu=\begin{cases}3.66 & \text{if } \frac{L}{D_{ut,i}}>0.055RePr\\ 1.86(RePr)^{\frac{1}{3}}\left(\frac{D_{ut,i}}{L}\right)^{\frac{1}{3}}\left(\frac{\mu_b}{\mu_w}\right)^{0.14} & \text{otherwise}\end{cases}, \quad (37)$$

$$St=0.023Re^{-0.2}Pr^{-\frac{2}{3}}\left(\frac{\mu_b}{\mu_w}\right)^{0.14}, \quad (38)$$

where $D_{ut,i}$ is the inner diameter of the fluid U-tube, and μ_b and μ_w are the HTF viscosity in the bulk and at the wall of the U-tube. The convective heat transfer coefficient is calculated for the relevant regime,

$$h_{cv,ct-HTF}=\begin{cases}\frac{k_{HTF}Nu}{D_{ut,i}} & \text{if } Re<3000\\ \frac{4Stm_{ETA}c}{\pi D_{ut,i}^2} & \text{otherwise}\end{cases}. \quad (39)$$

3.5. ORC sub-system model

The HTF from the ETAs is held up in the insulated TES hot tank. The tank outlet flow rate is continuous, enabling consistent loading and constant operation of the ORC sub-system. The outlet mass flow rate, m_{TES}, is expressed as the average of the mass flow rate in the ETAs over each hour of the day,

$$m_{TES}=\frac{\sum_{h=1}^{24}m_{ETA,h}}{24}. \quad (40)$$

The equations presented in Table 7 compute the variables required to model the performance of the ORC sub-system [68], with working fluid properties obtained from NIST REFPROP.

3.6. Water heaters

The models for HX1 and HX2 are analogous, where the mass flow rate of water, m_w, is varied to achieve a maximum temperature of 60 °C, the temperature at which water is typically stored for domestic hot water and space heating purposes [69]. Where the hot fluid temperature is below 60 °C plus the minimum approach temperature difference, the maximum theoretical temperature is attained. The water mass flow rate, m_w, is calculated from,

$$m_w=\frac{m_i c(T_i-T_{cold})}{c_w(T_{w,out}-T_{w,in})}, \quad i=\text{PVT or ETA} \quad (41)$$

where $T_{w,out}$ is the water outlet temperature, the and the water inlet temperature, $T_{w,in}$, is assumed equivalent to the ambient temperature. The temperature of the cold tank, T_{cold}, is assumed to be 5 °C higher than the ambient temperature. The HX thermal output, Q_{HX}, is calculated from,

Table 7
Summary of ORC sub-system modelling equations.

Component	Equation
Pump outlet specific enthalpy	$\dot{h}_{out,p}=\dot{h}_{in,p}+(\dot{h}_{out,p,s}-\dot{h}_{in,p})/\eta_p$
Expander outlet specific enthalpy	$\dot{h}_{out,exp}=\dot{h}_{out,evap}-\eta_{exp}\left(\dot{h}_{out,evap}-\dot{h}_{out,exp,s}\right)$
Working fluid mass flow rate	$m_{ORC}=\frac{m_{TES}c(T_{out,ETA}-T_{in,HX2})}{(\dot{h}_{out,evap}-\dot{h}_{in,evap})}$
Electricity generation	$E_{ORC}=m_{ORC}\left(\eta_{gen}\left(\dot{h}_{out,evap}-\dot{h}_{out,exp}\right)-\left(\dot{h}_{out,p}-\dot{h}_{in,p}\right)\right)$
Electrical efficiency	$\eta_{ORC}=\frac{\eta_{gen}\left(\dot{h}_{out,evap}-\dot{h}_{out,exp}\right)-\left(\dot{h}_{out,p}-\dot{h}_{in,p}\right)}{\dot{h}_{out,evap}-\dot{h}_{in,evap}}$

$$Q_{HX} = m_w c_w \left(T_{w,out} - T_{w,in}\right), \quad (42)$$

3.7. Technical performance parameters

The total system electricity generation, E_{total}, is calculated as a sum of the electricity generation from the ORC sub-system, E_{ORC}, and PV cells, E_{PV}, minus the sum of each pump's power consumption, $\dot{W}_{cp}$,

$$E_{total} = E_{ORC} + E_{PV} - \sum_{i=1}^{3} \dot{W}_{cp,i}. \quad (43)$$

The total thermal output of the system, Q_{total}, is a sum of the heat output in HX1, Q_{HX1}, and HX2, Q_{HX2},

$$Q_{total} = Q_{HX1} + Q_{HX2}. \quad (44)$$

The equivalent electricity generation, E_{equiv}, is calculated using a thermal-electrical equivalency factor of 0.55 in this study [70],

$$E_{equiv} = E_{total} + 0.55 Q_{total}. \quad (45)$$

The system electrical, $\eta_{el,sys}$, and thermal efficiency, $\eta_{th,sys}$, are defined as the ratio of total output relative to the solar energy incident on the PTC,

$$\eta_{el,sys} = \frac{E_{total}}{\gamma A_{PTC} G_{AM1.5}}, \quad (46)$$

$$\eta_{th,sys} = \frac{Q_{total}}{\gamma A_{PTC} G_{AM1.5}}. \quad (47)$$

3.8. Costing models

System costs are estimated from empirical correlations extrapolated from commercial product data, as presented in Table 8. These correlations are adjusted to account for inflation and assumptions are made conservatively where relevant.

Brazed plate heat exchangers are selected, as a common choice for commercial ORC systems, employed by various experimental systems due to their availability, low cost and sizes [71]. The heat transfer area, A_i, is calculated from,

$$A_i = \frac{Q_i}{U_i LMTD_i}, i = \text{HX1, HX2, evap, cond, reg} \quad (48)$$

Table 8
System costing equations.

Component	Unit	Cost, £	Ref.
Heat exchanger	A (m^2)	$177 + 289A$	[72]
ORC pump	$\dot{W}_p$ (W)	$308 + 0.62\dot{W}_p$	[72]
Expander	$\dot{W}_{exp}$ (kW)	1034, if $\dot{W}_{exp} < 1.9$kW; $649 + 192\dot{W}_{exp}$, otherwise	[73]
Generator	$\dot{W}_{exp}$ (kW), η_{gen} (%)	$3.869 \times 10^6 \left(\frac{\dot{W}_{exp}\eta_{gen}}{11800}\right)^{0.94}$	[44]
Battery	E_{PV} (kWh_{el}/day)	$128E_{PV}$	[74]
ORC working fluid	m_{ORC} (kg/h)	$20m_{ORC}$	[75]
Circulation pump	$\dot{W}_{exp}$ (W)	$80 + 0.6\dot{W}_{cp,i}$	[76]
PVT/ETA fluid	m_{PVT}, m_{ETA} (kg/s)	$3.9(3600m_{PVT} + 20000m_{ETA})$	[77]
Hot tank	V_{HT} (L)	$5159V_{HT}$	[72]
Cold tank	V_{HT} (L)	$56.4 + 0.35V_{CT}$	[78]
PVT tube	A_{PTC} (m^2), E_{PV} (W)	$228A_{PTC} + 1.2E_{PV}$	[79]
PTC & ETA	A_{PTC} (m^2)	$148.7A_{PTC}$	[80]
SBS filter	A_F (m^2)	$744A_F$	–

where U_i is the overall heat transfer coefficient and $LMTD_i$ is the log mean temperature difference across the heat exchanger.

The circulation pump cost is a function of power requirement, $\dot{W}_{cp,i}$, (the sum of assumed pressure drops due to bends, valves and heat exchangers, ΔP_{drop}, and the dynamic pressure requirement, $0.5\rho u^2$) at the maximum mass flow rate, m_{max},.

$$\dot{W}_{cp,i} = \frac{m_{max}}{\rho}\left(0.5\rho u^2 + \Delta P_{drop}\right), i = 1,2,3 \quad (49)$$

The hot tank and cold tank volumes, V_{HT} and V_{CT}, are estimated to store a day's worth of fluid, rounded to the nearest 50 L,

$$V_{HT} = V_{CT} = 86400 m_{TES}. \quad (50)$$

Relevant spectral beam splitting interference filter pricing data is limited, as they are not yet commercialised for solar energy systems and only that for very small-area applications has been reported. The filter cost is thus conservatively assumed equivalent to the combined PTC and ETA costs.

The total capital cost, C_{capex}, is determined as a sum of component costs, C_i, plus installation costs (assumed 16% of component costs), and operating costs, $C_{O\&M}$, are approximated as 1% of C_{capex} [40,42],

$$C_{capex} = \sum C_i + 0.16 \sum C_i, \quad \text{where } i = \text{all components} \quad (51)$$

$$C_{O\&M} = 0.01 C_{capex}. \quad (52)$$

3.9. Economic performance parameters

Annual net savings, NS, is calculated based on the displacement of electricity and natural gas, with respective energy prices, PR_{el} and PR_{gas}, presented in Table 5,

$$NS = E_{total} PR_{el} + Q_{total} PR_{gas} - C_{O\&M}, \quad (53)$$

where E_{total} and Q_{total} are the total electricity generation and thermal output in kWh/year. Government incentives for renewable generation are not considered due to significant variability with location.

Considering a discount rate, DR, of 5% [81] and an inflation rate, IR, of 1.23% [82], the system payback period, PBT, is calculated from,

$$PBT = \frac{\ln\left(1 + \frac{C_{capex}(IR-DR)}{NS}\right)}{\ln\left(\frac{1+IR}{1+DR}\right)}. \quad (54)$$

Assuming a total lifetime, n, of 25 years, the levelised cost of electricity, $LCOE_{el}$, is expressed as,

$$LCOE_{el} = \frac{C_{capex} + \sum_{n=1}^{25} C_{O\&M}(1+IR)^{n-1}(1+DR)^{-n}}{\sum_{n=1}^{25} \dot{E}_{total}(1+DR)^{-n}}. \quad (55)$$

4. Results and discussion

4.1. Operational parametric analysis

Parametric analysis is undertaken to provide insight into the optimal design and operation of the proposed SBS-CPVT-ORC system. The effects of varying the SBS optical filter cut-off wavelengths, PVT flow rate, ORC working fluid selection, ETA outlet temperature set point and ORC evaporation temperature, on the system's techno-economic performance are studied, with salient results presented below.

4.1.1. SBS filter cut-off wavelengths

Increasing the transmissive range of the SBS filter increases the fraction of total incoming solar irradiance transmitted via the filter to the PV cells. However, this also reduces the solar energy fraction reflected onto the ETA, which in turn acts as the heat source to the ORC sub-system that generates secondary electrical power. A trade-off hence exists in the hybrid system, resulting from the optimal division of the

solar spectrum between the PVT tube and ETA. The effects of simultaneously varying the lower and upper cut-off wavelengths of the SBS filter (i.e., λ_{min} and λ_{max}) on the PV cell efficiency, $\eta_{el,PV}$, and the total system electricity generation, E_{total}, are shown in Figs. 5 and 6.

Interestingly, Figs. 5 and 6 show that $\eta_{el,PV}$ and E_{total} are maximised when the upper limit is around 860 nm, which corresponds to the bandgap wavelength of GaAs PV cells. This value agrees well with existing literature where the optimal upper limit of the SBS filter for GaAs PV cells was also found to be around 860 nm [27]. When considering the total (combined) system electricity generation from the PV cells and ORC sub-system, the optimal transmissive range is approximately 485–860 nm. In this study, the transmissive range of the SBS filter was selected to be 485–860 nm to achieve a satisfactory system electrical performance. This results in the filter transmitting ~47% of incident solar energy onto the PV cells and reflecting the other ~53% of solar energy onto the ETA, with zero energy loss due to the idealised SBS filter model (see Section 3.2).

4.1.2. Flow rate in the PVT tube

The HTF flowing through the PVT tube improves the PV electrical efficiency by removing heat from the cells, which is then utilised for providing hot water for direct use and space heating. Increasing the flow rate significantly reduces the PV cell temperature, which increases PV efficiency, with a diminishing effect after ~20 kg/h, as shown in Fig. 7.

For a constant solar irradiance, G, increased efficiency gives rise to a proportional increase in electricity generation, as shown in Fig. 8. Reducing the flow rate, however, leads to an almost linear reduction in HX1 thermal output, thus it is not optimal to use the highest flow rate possible. In this study, a flow rate of 32.4 kg/h is selected as a good balance between the electrical and thermal energy generation.

4.1.3. ETA outlet temperature and ORC sub-system operation

The HTF flow rate in the ETA varies relative to the solar intensity to maintain the specified set point of the ETA outlet HTF temperature, $T_{out,ETA}$. This set point determines the flow rate and temperature of HTF delivered to the ORC sub-system from the TES tank, thus impacting the electricity generation of the ORC sub-system. The practical ranges of the HTF temperature at the ETA outlet and ORC evaporation temperatures are studied for a range of different ORC working fluids. The maximum ETA outlet HTF temperature attained in this study is 360 °C, while maintaining reasonably high flow rates through the ETA. Of the ORC working fluids evaluated, Toluene is selected for the subsequent parametric analyses, with a high critical temperature (319 °C) complementary to the high HTF temperatures attained in the ETA, enabling higher efficiency and electricity generation.

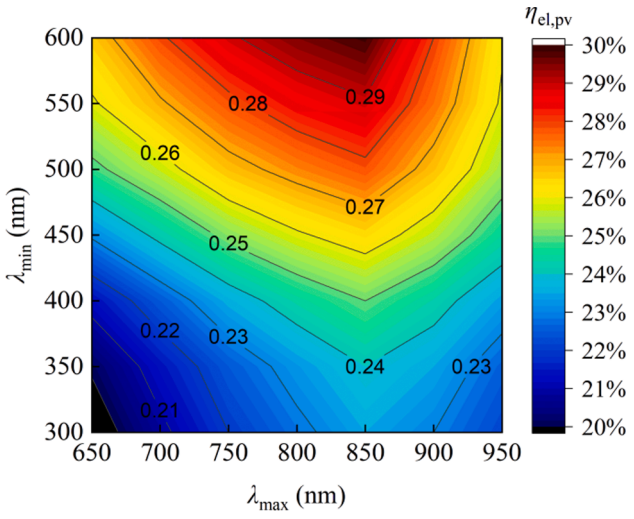

Fig. 5. PV cell electrical efficiency in Spain with different SBS filter cut-off wavelengths.

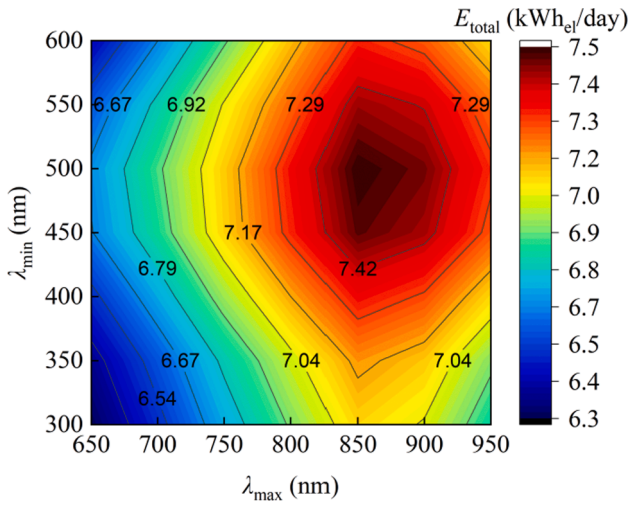

Fig. 6. Total PV and ORC electricity generation in Spain with different SBS filter cut-off wavelengths.

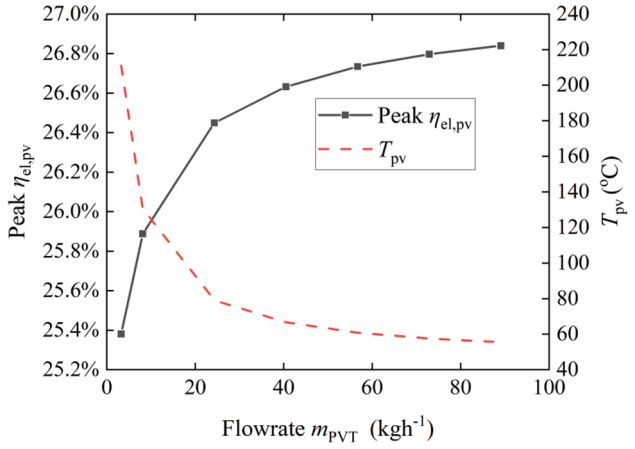

Fig. 7. PV temperature and efficiency in Spain as a function of PVT flow rate. The SBS filter transmissive window is fixed at 485–860 nm.

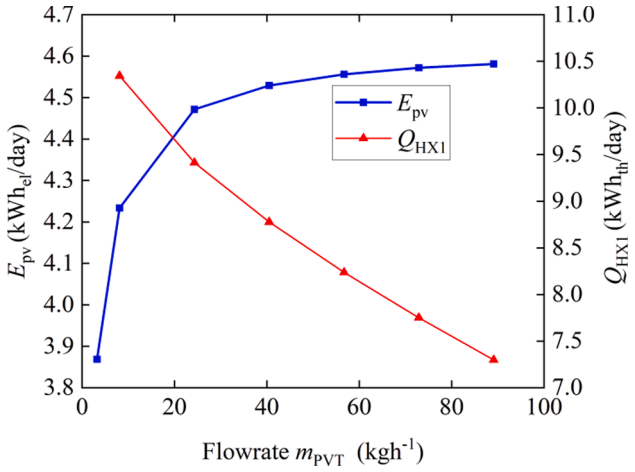

Fig. 8. PV electricity generation and HX1 thermal output in Spain as a function of PVT flow rate. The SBS filter transmissive window is fixed at 485–860 nm.

Fig. 9 shows the respective impact of varying the evaporation temperature, $T_{out,evap}$, on the system's net electricity and thermal

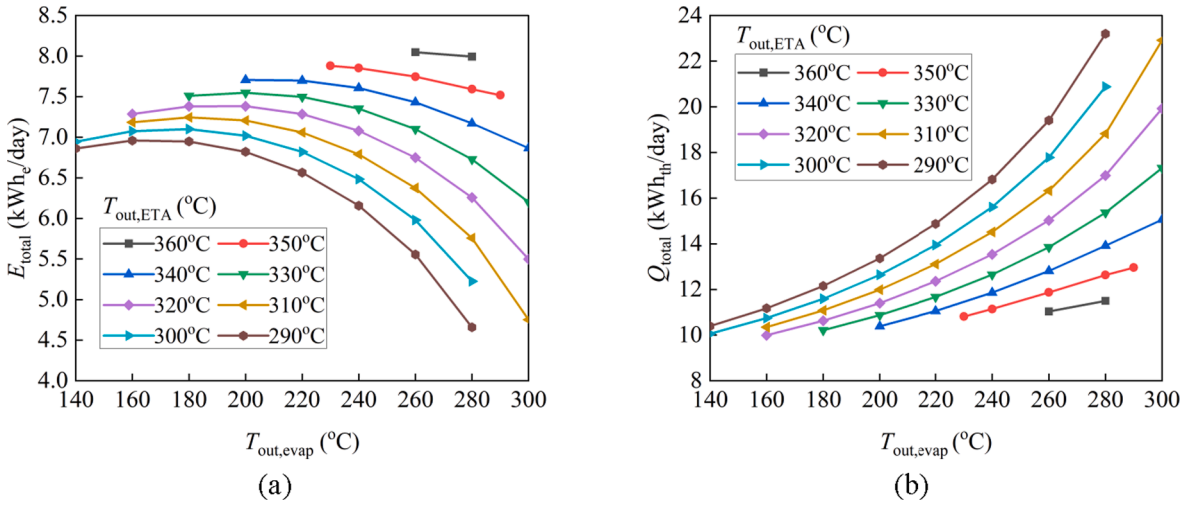

Fig. 9. (a) System electricity generation, E_{total}, and, (b) system thermal output, $Q_{total,}$ as a function of ORC evaporation temperature, $T_{out,evap}$, with different ETA outlet HTF temperatures in Spain, using Toluene as the working fluid. The SBS filter transmissive window is fixed at 485–860 nm.

generation, for different ETA outlet HTF temperatures, $T_{out,ETA}$. For context, the output from the PV cells and HX1 are constant at 4.51 kWh$_{el}$/day and 8.19 kWh$_{th}$/day, respectively. For a given evaporation temperature, increasing $T_{out,ETA}$ enables higher evaporator heat transfer rates and thus larger ORC flow rates, resulting in a higher electricity generation. For a fixed ETA outlet temperature, as $T_{out,evap}$ increases, a maximum output of the ORC sub-system is reached, after which it diminishes, since the ORC efficiency increases, while the ORC working fluid flow rate simultaneously decreases. Increasing $T_{out,evap}$ increases the temperature of the fluid exiting the hot side of the evaporator, subsequently increasing the thermal output of HX2. Increasing the $T_{out,ETA}$ reduces the flow rate of the hot-side fluid, thus reducing energy available to HX2 for a fixed evaporation temperature.

Fig. 10 shows that the system's $LCOE_{el}$ is inversely proportional to the electricity generation of the ORC sub-system shown in Fig. 9. This is because, over the range of conditions studied, the change in capital cost is small relative to the change in electricity generation, and hence the $LCOE_{el}$ is minimised where generation is the highest. The payback time, *PBT*, decreases with higher evaporation temperatures because, despite decreasing the ORC power output, the delivered thermal energy increases, resulting in an overall rise in net energy savings for the electricity-to-gas price ratio modelled for Spain. Simultaneously, component capacities are reduced due to lower ORC working fluid flow rates at higher evaporation temperatures, leading to a small reduction in capital cost. The operating point selected for the remaining techno-economic analyses is at an ETA and evaporation temperature of 360 °C and 260 °C, respectively, to maximise electricity generation and minimise the $LCOE_{el}$.

4.2. System-scale analysis

To analyse the economic potential of this system, the system's performance is simulated at various scales/capacities. The system capacity is increased by fixing the design and operational parameters of the collectors, while only increasing the number of solar collectors and thus the total PTC area. The ORC sub-system and HX2 capacities remain reactive to the flow rate and temperature from the hot tank. The resulting linear change in electricity and thermal output as a function of total PTC area is presented in Fig. 11, where the system ratio of heat to power is maintained at 1.36 to achieve the maximum electricity generation, comparable to gas turbines and other common CHP systems [53,54].

This study explores the potential of exploiting SBS-CPVT-ORC systems as a competitive, small-scale CHP option for the domestic/

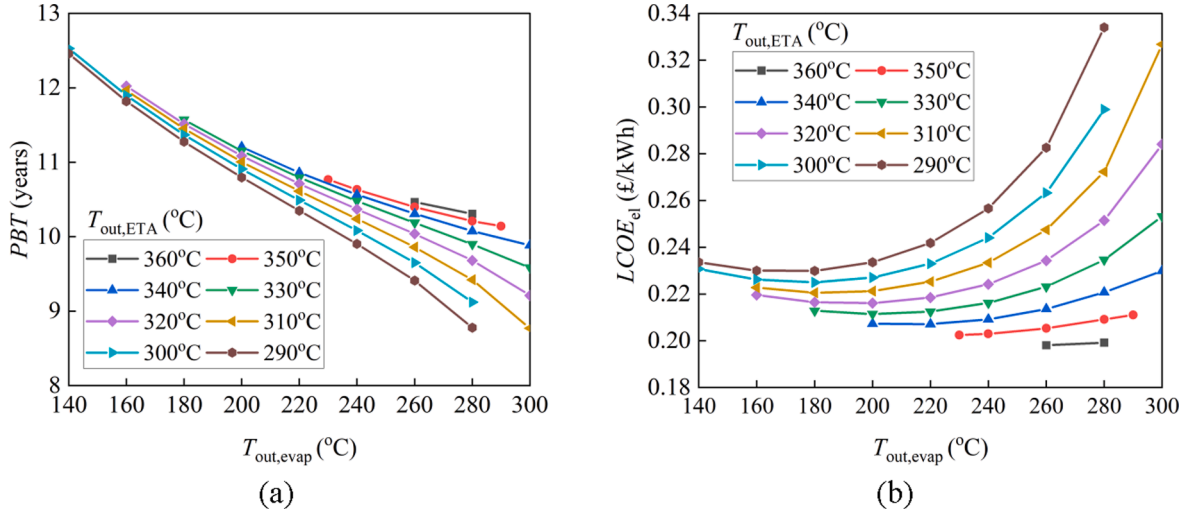

Fig. 10. (a) *PBT*, and, (b) levelised cost of electricity, $LCOE_{el}$, as a function of ORC evaporation temperature, $T_{out,evap}$, with different ETA outlet HTF temperatures in Spain, using Toluene as the working fluid. The SBS filter transmissive window is fixed at 485–860 nm.

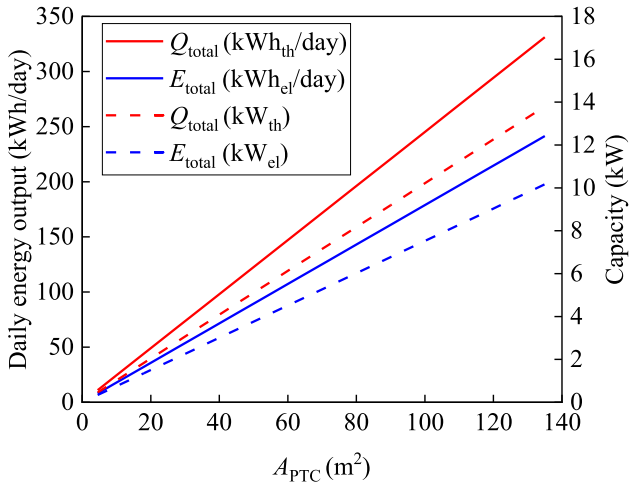

Fig. 11. System electricity and thermal output in Spain as a function of PTC area. The ETA outlet temperature and ORC evaporation temperature are set to 360 °C and 260 °C, respectively, with Toluene as the ORC working fluid. The SBS filter transmissive window is fixed at 485–860 nm.

residential sectors. Given this focus, we set the upper limit of the generation capacity of the systems to be 10 kW$_{el}$, which is typical for domestic/residential applications. The variation of the technical and economic performance of the systems over the capacity range from 1 to 10 kW$_{el}$ is investigated in this study. Fig. 12 shows a corresponding linear increase in system capital cost with capacity, with the number of houses this would fully supply with electricity in Spain shown for reference. At a capacity of 0.2 kW$_{el}$ (PTC area of 4.5 m^2), the capital cost per house supplied is ~£9000. As the capacity increases, the cost per house supplied reduces, reaching ~£4600 per house at capacities >3.6 kW$_{el}$ (PTC areas >100 m^2).

Fig. 13 shows the cost breakdown of the whole system and of the ORC sub-system. The solar field components account for a large proportion of the cost, increasing from ~22% to ~43% at larger system capacities. Under the conservative assumption that the SBS filter cost is equivalent to the combined cost of the PTC and ETA, this also forms a large part of the cost, reaching ~22% of the total capital expenditure.

Most notably, the ORC sub-system initially forms a significant 40% of

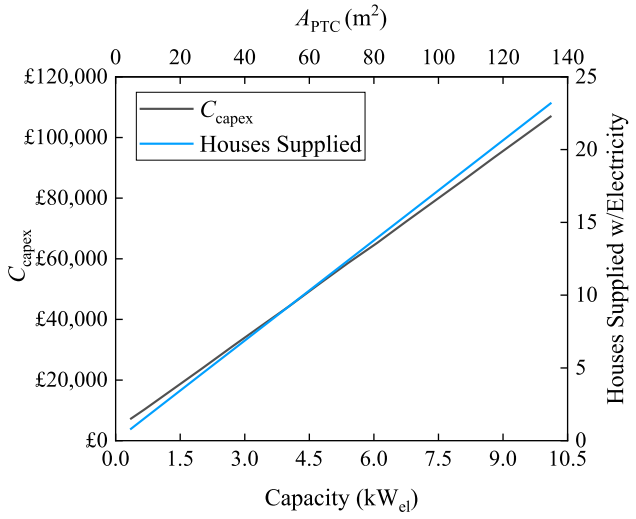

Fig. 12. Capital cost and number of houses supplied with electricity in Spain as a function of system capacity (bottom horizontal axis) and PTC area (top horizontal axis). The ETA outlet temperature and ORC evaporation temperature are set to 360 °C and 260 °C, with Toluene as the ORC working fluid. The SBS filter transmissive window is fixed at 485–860 nm.

the total cost, which sharply decreases to ~10% at larger capacities. This is partly because the ORC sub-system (and its components) benefits from economies of scale. For example, the lowest-rated scroll-type turbine available is ~1.8 kW, but the ORC power output only reaches 1.8 kW at ~45 m^2 PTC area in Spain, thus the turbine initially forms a disproportionate fraction of the cost. Also, based on the costing models presented, the solar collector costs increase at higher capacities (i.e., array areas) to a greater extent than the ORC sub-system. This suggests that integrating an ORC sub-system into the SBS-CPVT collector is more economically favourable at larger capacities, which will be further investigated in Section 4.4.

Fig. 14 shows the *PBT* and *LCOE*$_{el}$ for different system capacities in Spain. The system exhibits a significantly improved economic performance at larger capacities, with both *PBT* and *LCOE*$_{el}$ decreasing by approximately half. At larger solar collector areas, the total electricity and thermal outputs increase by more than the total cost, resulting in the observed steep decline in the *PBT* and *LCOE*$_{el}$. A desirable *PBT* (down to ~4–5 years) and *LCOE*$_{el}$ (~0.10 £/kWh) are attained thanks to Spain's good solar conditions, as well as comparatively high energy prices, leading to high energy savings and low *PBT*s. Notably, as capacity is increased beyond 10 kW$_{el}$, the impact on economic performance is slight, for example, increasing the capacity from 10 kW$_{el}$ to 500 kW$_{el}$ results in only a ~3% and ~2% change in *PBT* and *LCOE*$_{el}$, respectively.

As an emerging technology for solar systems, the SBS filter unit cost is assumed to be 744 £/m^2, i.e., equivalent to the PTC and ETA total, making up a large proportion of the total system cost. Fig. 15 shows the effect of the filter unit cost on the *PBT* and *LCOE*$_{el}$ at PTC areas of 4.5 m^2 and 45 m^2 (capacities of 0.3 kW$_{el}$ and 3.4 kW$_{el}$, respectively). These areas are chosen as they represent the smallest modelled collector area, and the area after which economic benefits from a further increasing area are diminished. Reducing the optical SBS filter cost benefits both the *PBT* and *LCOE*$_{el}$ similarly at all system capacities, with the filter accounting for a *PBT* increase of about 1–1.5 years between a unit cost of 0 and 744 £/m^2.

4.3. Regional analysis

In previous sections, system performance was evaluated for Spain, however, it is important to assess techno-economic performance of this system at different climate conditions and for different economic factors. Therefore, the UK and Oman are considered as respective countries with lower and higher solar irradiance levels. The optimal lower cut-off wavelength of the SBS filter, which maximises the total electricity generation (the sum of PV and ORC electricity generation) in different locations, is 485, 485 and 500 nm for the SBS-CPVT-ORC systems in Spain, UK and Oman. Oman has a significantly higher solar irradiance than UK and Spain, resulting in a higher operating temperature and lower electrical efficiency of the PV cells. For the SBS-CPVT-ORC system in Oman, although the electricity generation from the PV cells slightly decreases when increasing the lower cut-off wavelength of the SBS filter from 485 nm to 500 nm, the ORC sub-system generates relatively more electricity by receiving more input thermal energy, which benefits the overall system performance. Therefore, the optimal lower cut-off wavelength of the SBS filter for Oman is slightly larger than that for UK or Spain. The PVT flow rate, ETA outlet temperature, ORC working fluid and evaporation temperature used for Spain are also kept unchanged. Key technical performance results that are sustained irrespective of system size are summarised in Table 9. As expected, the electrical and thermal outputs are directly correlated with solar irradiance levels, being lower in the UK and higher in Oman. The SBS-CPVT-ORC system achieves very good CHP performance in all regions studied. The improved performance from introducing a PTC and a SBS filter is demonstrated by comparing the PVT-ORC system (employing α-Si PV cells) proposed by Kutlu et al. [37], whose highest daily power output was 0.82 kWh$_{el}$/m^2 of solar-collector area, without the delivery of any thermal energy to the building or end user. A SBS-CPVT CHP system

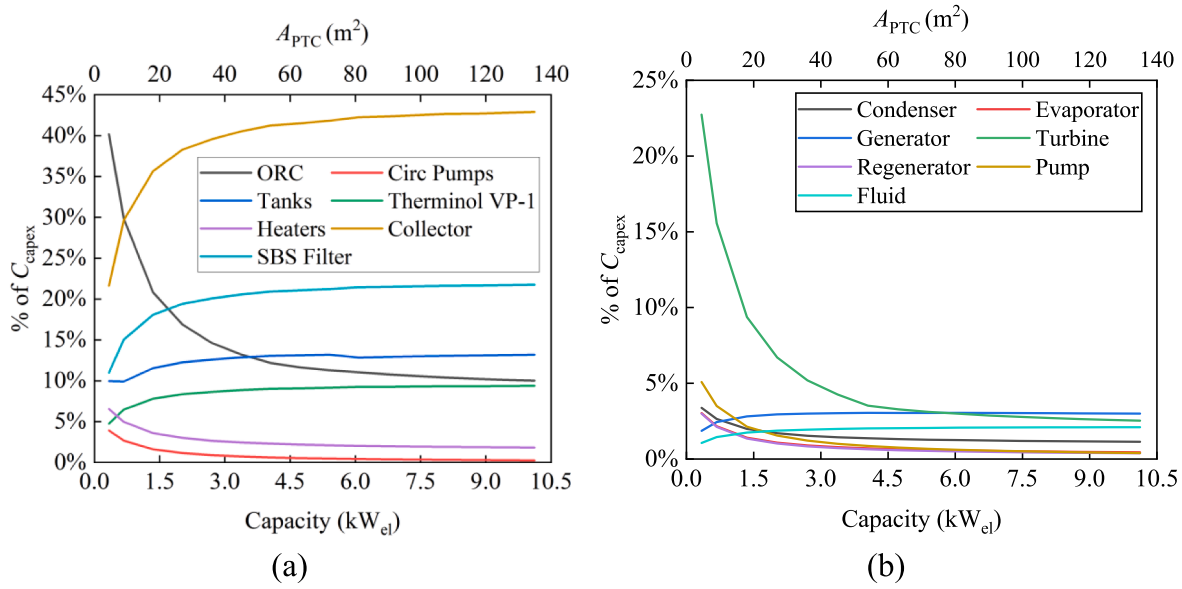

Fig. 13. Effect of capacity/PTC area on: (a) system component cost breakdown, and (b) ORC sub-system component cost breakdown, for the proposed system in Spain. The ETA outlet temperature and ORC evaporation temperature are set as 360 °C and 260 °C, with Toluene as the ORC working fluid. The SBS filter transmissive window is fixed at 485–860 nm.

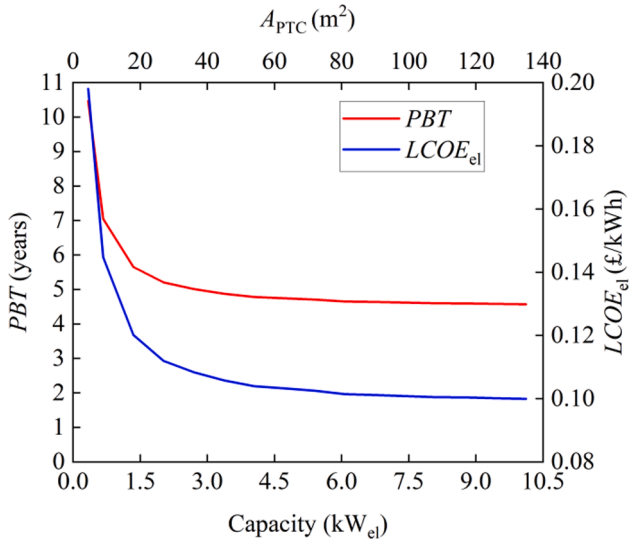

Fig. 14. *PBT* and $LCOE_{el}$ in Spain as a function of system capacity and PTC area. The ETA outlet temperature and ORC evaporation temperature are set as 360 °C and 260 °C, with Toluene as the ORC working fluid. The SBS filter transmissive window is fixed at 485–860 nm.

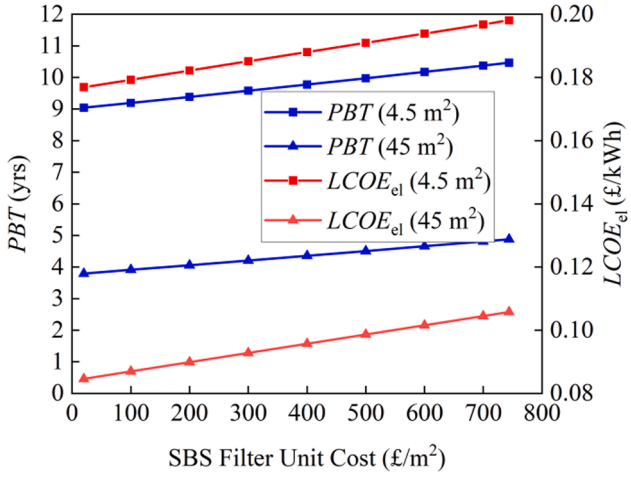

Fig. 15. System *PBT* and $LCOE_{el}$ as a function of SBS filter unit cost in Spain. The ETA outlet temperature and ORC evaporation temperature are set as 360 °C and 260 °C, with Toluene as the ORC working fluid. The SBS filter transmissive window is fixed at 485–860 nm.

with a similar design (employing Si PV cells) in Italy [26] was predicted as being able to deliver an average daily output of 0.13 kWh$_{el}$/m^2 and 0.85 kWh$_{th}$/m^2, compared to 0.95 kWh$_{el}$/m^2 and 1.17 kWh$_{th}$/m^2 achieved in the UK by the SBS-CPVT-ORC system proposed in the present study. This indicates that performance improvements can be achieved by integrating an ORC sub-system and using a high-performance GaAs-type PV cell.

Diurnal total electricity generation and thermal output (for the average daily solar profile in a year) is compared in Fig. 16. Constant baseline electricity and thermal generation are observed during the day, generated by the ORC sub-system and HX2, respectively. Additional electricity and heat are generated by the PVT tube and HX1 in the daytime, in proportion to the solar input.

System economic potential is not only related to the available solar resource at the installation region and the resulting energy output but also strongly depends on the national energy prices. As shown in Fig. 17, the $LCOE_{el}$ is inversely correlated with region solar irradiance, with a minimum attainable value of 0.09 £/kWh in Oman, and a minimum of 0.15 £/kWh in the UK. The system *PBT* in the UK is very high at the

Table 9
Comparison of key system characteristics for the considered regions.

Parameter	Spain	UK	Oman
Lower filter limit, λ_{min} (nm)	485	485	500
Upper filter limit, λ_{max} (nm)	860	860	860
Average, E_{total}/A_{PTC} (kWh$_{el}$/day/m^2)	1.80	0.95	2.05
Average, Q_{total}/A_{PTC} (kWh$_{th}$/day/m^2)	2.45	1.17	2.69
Ratio of heat to power	1.36	1.24	1.30
$\eta_{el,sys}$ (%)	23.5	23.6	23.6
$\eta_{th,sys}$ (%)	31.9	29.2	30.7

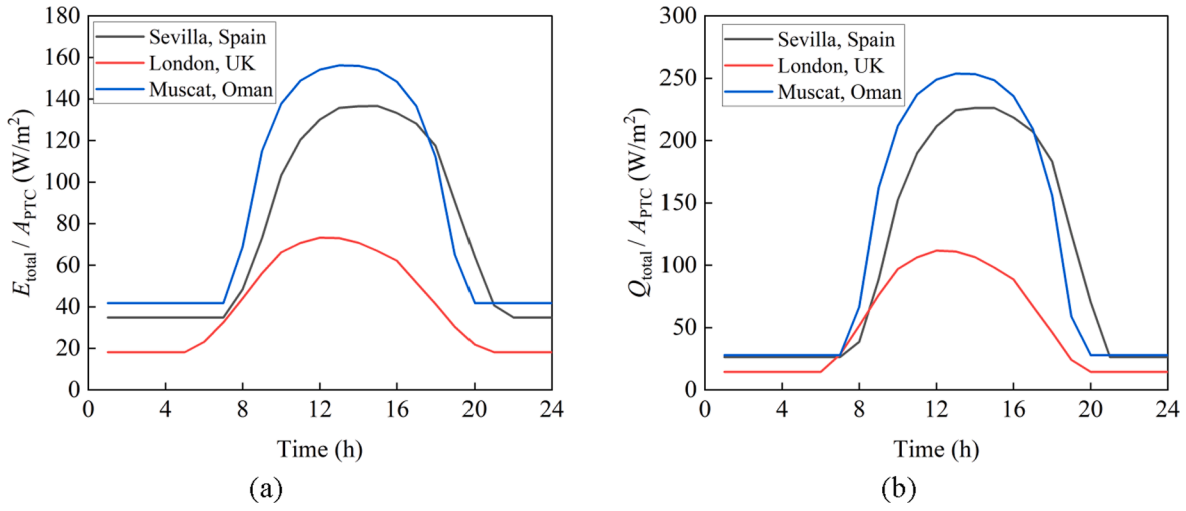

Fig. 16. (a) Electricity, and (b) thermal output unit per area of PTC over a 24-hour period in the considered regions. The ETA outlet temperature and ORC evaporation temperature are set to 360 °C and 260 °C, with Toluene as the ORC working fluid. The SBS filter transmissive window is fixed at 485–860 nm.

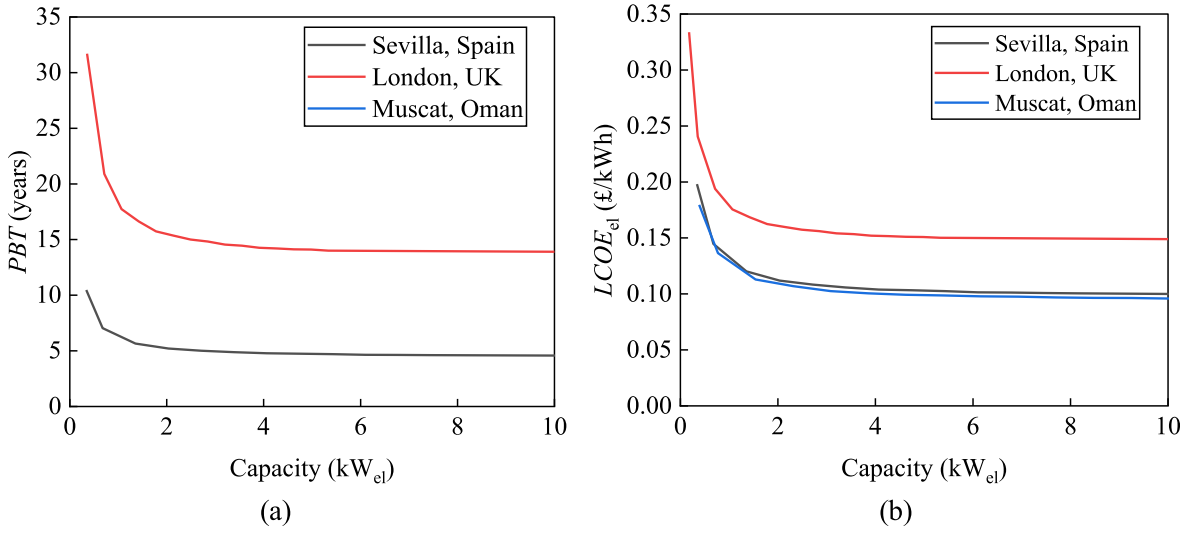

Fig. 17. (a) *PBT*, and (b) $LCOE_{el}$ as a function of system capacity in the considered regions. The ETA outlet temperature and ORC evaporation temperature are set as 360 °C and 260 °C, with Toluene as the ORC working fluid. The SBS filter transmissive window is fixed at 485–860 nm.

initial ~0.2 kW_{el} capacity (4.5 m^2 PTC area) studied, as a result of lower energy prices and lower irradiance. However, increasing the capacity to just ~0.8 kW_{el} (PTC area of 20 m^2) decreases *PBT* to <20 years in the UK, levelling off at ~14 years for larger capacities. These times are competitive with solar-PV systems in the UK, which typically pay back in 18–25 years (with incentives) [46,47], reaching as low as 8 years in some cases [87]. Despite Oman having the highest solar irradiance, system costs are not paid back at any capacity as Oman has some of the cheapest energy prices in the world. The operating conditions modelled here are chosen to maximise electricity generation, enabling a ratio of heat to power of 1.3, comparable to gas turbines and other common CHP systems [53,54].

The energy prices are, therefore, important factors that affect the financial potential of these systems, and as these are also inherently and highly variable, it is important to understand their influence on the system's *PBT*. Fig. 18 shows the impact of variable energy prices at a PTC area of 9 m^2 (capacity of ~0.7 kW_{el} in Spain and ~0.4 kW_{el} in the UK). For this area, using UK energy prices in both countries yields a *PBT* of 17 years in Spain, compared to 87 years in the UK, with these times respectively reducing to 10 and 23 years (not shown here) at an increased area of 45 m^2 (~3.4 kW_{el} in Spain and ~1.8 kW_{el} in the UK). This difference highlights the significant impact that solar irradiance has on the system's economic potential. For the capacity shown, using Spain's energy prices in the UK reduces *PBT* from 87 to 19 years, with times as low as 10 years attainable at a capacity of 1.8 kW_{el} (45 m^2), showing that highly competitive times can be attained even in relatively low irradiance regions.

Furthermore, Fig. 19 shows the impact of varying electricity prices and system capacity in Oman. Increasing the electricity price to 0.04 £/kWh results in system payback times of <16 years attained at electrical capacities over 3.9 kW_{el} (PTC area of 45 m^2). Using either UK or Spanish electricity prices yields paybacks of <5 years with capacities as small as 0.8 kW_{el} (9 m^2), demonstrating the exceptional potential of this CHP system in a maximum solar irradiance scenario.

4.4. System cost and environmental competitiveness

To assess the impact of integrating the ORC sub-system on the wider system's economic viability, Fig. 20 shows comparisons of the $LCOE_{el}$ of SBS-CPVT systems with/without the ORC sub-system at different

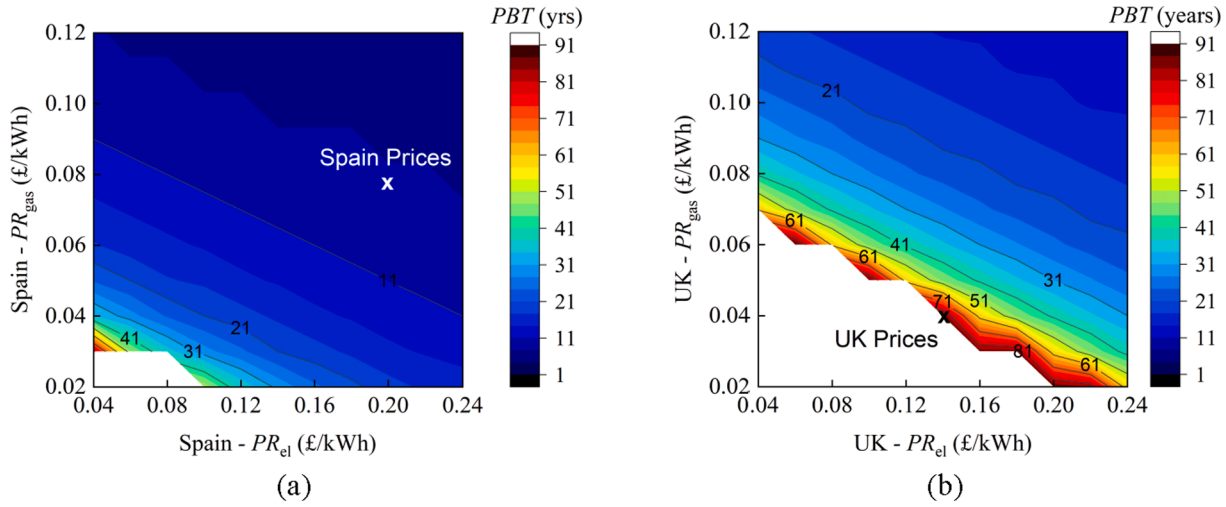

Fig. 18. Effect of gas and electricity prices on *PBT* of a system with a 9 m^2 PTC area in: (a) Spain, and (b) the UK. The ETA outlet temperature and ORC evaporation temperature are set to 360 °C and 260 °C, with Toluene as the ORC working fluid. The SBS filter transmissive window is fixed at 485–860 nm.

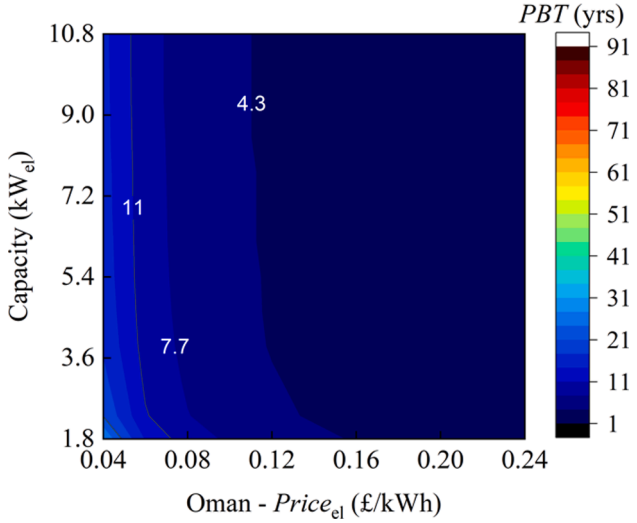

Fig. 19. System *PBT* in Oman at different system capacities and electricity prices. The ETA outlet temperature and ORC evaporation temperature are set to 360 °C and 260 °C, with Toluene as the ORC working fluid. The SBS filter transmissive window is fixed at 500–860 nm.

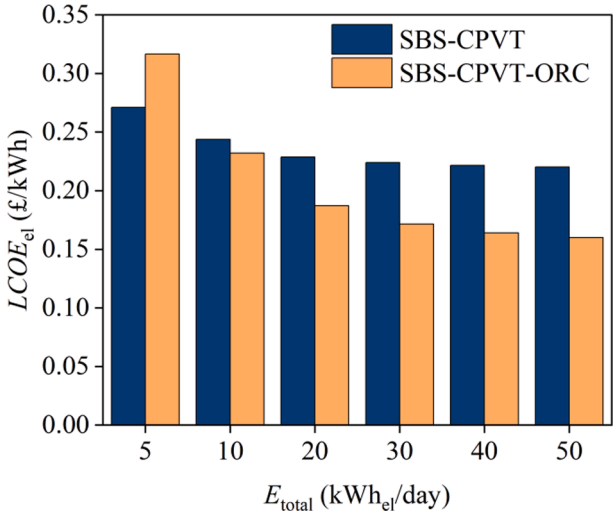

Fig. 20. System $LCOE_{el}$ with and without ORC integration in the UK.

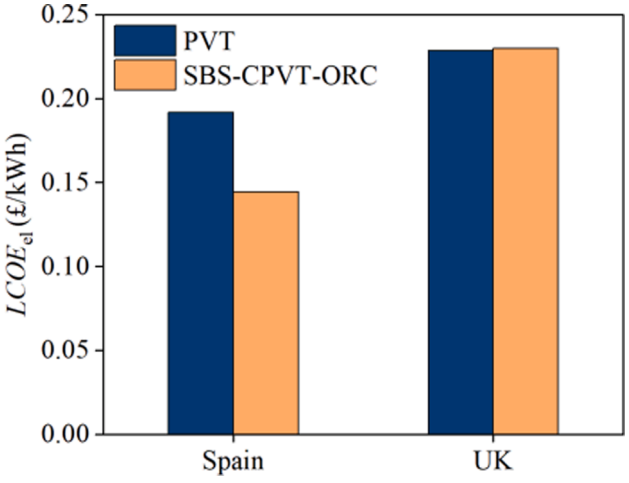

Fig. 21. Comparison of $LCOE_{el}$ for the proposed SBS-CPVT-ORC system and a PVT-CHP system [10] in Spain and the UK.

electrical output capacities in the UK. The comparison is modelled by removing the ORC sub-system and increasing the SBS filter transmissive range to 400–900 nm to maximise PV electricity generation. Other characteristics are maintained the same as the combined SBS-CPVT-ORC system. At an output of 5 kWh_{el}/day, removing the ORC sub-system is the better option, suggesting that at such small capacities the electricity generated by the ORC sub-system is not worth the additional capital cost. Despite this higher initial cost, it is evident that integrating an ORC sub-system with the SBS-CPVT collector enables greater economies of scale. Increasing the output to just 10 kWh_{el}/day results in a lower $LCOE_{el}$ for the SBS-CVPT-ORC system, with the $LCOE_{el}$ being >27% lower at outputs >50 kWh_{el}/day.

The $LCOE_{el}$ of the proposed SBS-CPVT-ORC system is compared to a domestic PVT-CHP system proposed by Herrando et al. [10], which consists of a PVT collector, thermal storage tank and auxiliary heater and produces 3487 kWh_{el}/year in Zaragoza, Spain, and 3025 kWh_{el}/year in London, UK. For comparison, the SBS-CPVT-ORC system's $LCOE_{el}$ is taken at the scale with the same electricity generation, using the same inflation and depreciation rates, while the PVT-CHP system's

$LCOE_{el}$ is adjusted for a 2020 monetary value. Fig. 21 shows that the $LCOE_{el}$ is almost identical in the UK. At higher solar irradiance conditions in Spain, the SBS-CPVT-ORC system's $LCOE_{el}$ is lower by almost 0.05 £/kWh. It should also be noted that the PVT-CHP system generates less thermal energy, with a ratio of heat to power of 0.46 and 0.54 for Zaragoza and London, respectively, while that of the SBS-CPVT-ORC system is 1.36 and 1.24. Hence, considering that the total energy output (and since the SBS system has a thermal output 3 times larger), the SBS-CPVT-ORC system is attractive in both locations.

To give further context to the proposed system's economic performance and ultimate potential, the $LCOE_{el}$ is benchmarked against alternative CHP technologies. Fig. 22 compares data for common non-solar CHP types [88] against the $LCOE_{el}$ attained in the UK and Spain at a PTC area of 50 m^2 (~2 kW_{el} in the UK and ~3.8 kW_{el} in Spain), after which there is minimal benefit from increasing scale further. In addition to the advantage of supplying renewable energy, the proposed system is competitive with established CHP technologies. The SBS-CPVT-ORC system is shown to be a promising CHP technology under higher solar irradiance conditions in Spain.

Finally, Table 10 summarises the environmental benefits of these system in terms of emission reductions from displacing current residential space and water heating technologies in the UK. Conservatively assuming that 85% of the heat is delivered through gas boilers [89], and the remaining is electrical heating, potential emissions reductions from using such solar-based systems are significant, further demonstrating the potential as a competitive technology option for decarbonising the buildings sector.

5. Conclusions

A solar-CHP system, that integrates SBS-CPVT collectors with an ORC sub-system, has been assessed from both technical and economic perspectives. The design implements a PTC, concentrating light onto a SBS filter which transmits a specified band of spectral irradiance onto the PVT tube for electricity and heat generation. A HTF cools the PV (specifically, GaAs) solar cells, improving their electrical efficiency and co-generating thermal energy for the provision of domestic hot water and space heating. The remaining portion of spectral irradiance is reflected by the SBS filter onto an ETA, generating high-temperature thermal energy (set-point of up to 360 °C) in a separate fluid loop. This high-temperature fluid feeds a TES system, allowing constant loading/operation of the ORC sub-system, with excess heat also used for the provision of domestic hot water and space heating.

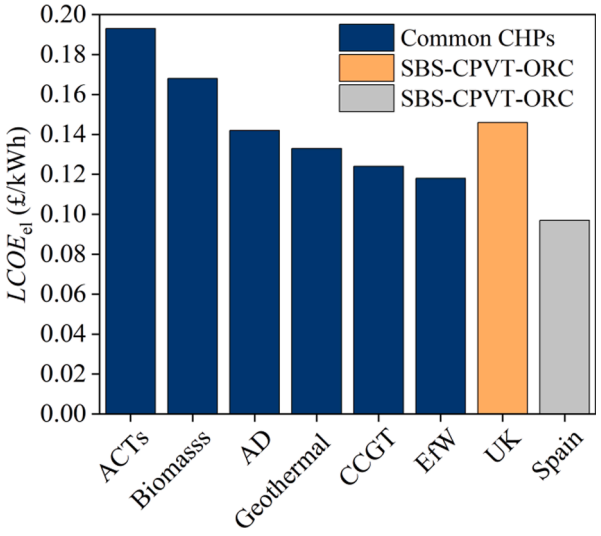

Fig. 22. Comparison of $LCOE_{el}$ for common non-solar CHP types. Utilises central estimate of CHP projects commissioning in 2025 [88]. ACT: advanced conversion technologies, such as gasification; AD: anaerobic digestion; EfW: energy from waste; CCGT: combined cycle gas turbine.

Table 10
Comparison of key system characteristics for the considered regions.

Parameter	Range	Ref.
Average 2021 grid intensity (gCO_2e/kWh)	211	[90]
Gas boiler intensity (gCO_2e/kWh)	210–380	[91]
UK residential heating intensity (gCO_2e/kWh)	210–355	
Solar thermal intensity (gCO_2e/kWh)	10–35	[91]
Emissions reduction using solar (%)	83–97	

This system is unique as the SBS filter splits the solar spectrum between the PV cells and ORC sub-system, thus the transmissive range is carefully chosen to optimise the overall electrical performance. Parametric analyses show that both the PV efficiency and the total system electricity generation are maximised when the upper transmissive limit of the SBS filter is ~860 nm. A lower limit of 600 nm enables the maximum PV efficiency, while ~500 nm maximises total system electricity generation.

For all regions studied (Spain, the UK and Oman), the electricity generation of the ORC sub-system is maximised for the highest ETA outlet temperature set point of 360 °C, when using Toluene as the working fluid and an evaporation temperature of 260 °C. With design parameters set to maximise the system total electrical performance, a ratio of heat to power of ~1.3 is attained, which is comparable to gas turbines and other conventional CHP systems. This translates to system electrical and thermal efficiencies of ~24 % and 31%, respectively. Approximately 54% of electricity is generated by the PV cells, with the rest generated by the ORC sub-system. Electricity generation of 1.8, 0.9 and 2.1 kWh_{el}/day per m^2 of PTC area is achieved in Spain, the UK and Oman, respectively, showing the strong dependence of thermodynamic performance on incident solar irradiance.

Increasing the overall capacity of the system through the use of larger solar collector areas, and hence the PV and ORC electrical outputs, improves economic performance significantly, with improvement diminishing after ~25 m^2 PTC area (equating to 44.7, 23.4 and 50.8 kWh_{el}/day in Spain, the UK and Oman,), suggesting a lower suitability as small/single household CHP systems. In Spain, a highly desirable *PBT* of <5 years is obtainable due to the high solar irradiance and energy prices. In the UK, competitive paybacks below 14 years can be attained despite the relatively low solar irradiance, showing great economic potential. Energy prices are pivotal to the system's economic viability, with an assumed price of just 0.04 £/kWh_{el} resulting in a *PBT* below 16 years in Oman.

In the UK, a $LCOE_{el}$ of 0.15 £/kWh (achieved at >3 kW_{el}) is shown to be highly competitive, with $LCOE_{el}$ values ranging between 0.12 and 0.19 £/kWh for established non-solar conventional CHP systems. Spain's higher solar irradiance results in a $LCOE_{el}$ of 0.10 £/kWh at capacities over 4 kW_{el}, outperforming alternative solutions. Compared to a simple PVT-CHP system with the same output, the $LCOE_{el}$ is almost identical in the UK, while in Spain the $LCOE_{el}$ is 24% lower for the SBS-CPVT-ORC system. Interestingly, at outputs above 5 kWh_{el}/day (~5.5 m^2 PTC area in the UK), the $LCOE_{el}$ of the SBS-CPVT-ORC system is shown to be superior to a SBS-CPVT system, suggesting that the integration of an ORC sub-system is not economically feasible at very small capacities but enables appreciable benefits from economies of scale. The results presented in this paper demonstrate significant potential for the proposed system to be a high efficiency, economically competitive, renewable alternative to combustion-based CHP systems.

CRediT authorship contribution statement

Joshua Peacock: Conceptualization, Methodology, Validation, Formal analysis, Investigation, Writing – original draft, Writing – review & editing. **Gan Huang:** Conceptualization, Methodology, Validation,

Writing – review & editing. **Jian Song:** Conceptualization, Methodology, Validation, Writing – review & editing. **Christos N. Markides:** Conceptualization, Methodology, Resources, Writing – review & editing, Supervision, Project administration.

Declaration of Competing Interest

The authors declare that they have no known competing financial interests or personal relationships that could have appeared to influence the work reported in this paper.

Data availability

Data will be made available on request.

Acknowledgements

This work was supported by the UK Engineering and Physical Sciences Research Council (EPSRC) [grant numbers EP/M025012/1, and EP/R045518/1]. The work was also supported by the Royal Society via an International Collaboration Award 2020 [grant number ICA\R1 \201302]. The authors would like to thank UK company Solar Flow Ltd. (www.solar-flow.co.uk). Data supporting this publication can be obtained on request from cep-lab@imperial.ac.uk. For the purpose of Open Access, the authors have applied a CC BY public copyright licence to any Author Accepted Manuscript version arising from this submission.

References

[1] BP Energy, "Energy Outlook 2020," *BP Energy Outlook 2030, Stat. Rev. London Br. Pet.*, p. 81, 2020, [Online]. Available: https://www.bp.com/content/dam/bp/business-sites/en/global/corporate/pdfs/energy-economics/energy-outlook/bp-energy-outlook-2020.pdf.

[2] International Energy Agency, "Global Energy Review 2021," 2021. doi: 10.1787/a60abbf2-en.

[3] Oyewunmi OA, Kirmse CJW, Pantaleo AM, Markides CN. Performance of working-fluid mixtures in ORC-CHP systems for different heat-demand segments and heat-recovery temperature levels. Energy Convers Manag 2017;148:1508–24. https://doi.org/10.1016/j.enconman.2017.05.078.

[4] US Environmental Protection Agency, "Discover CHP | Combined Heat and Power (CHP) Partnership." https://www.epa.gov/chp/discover-chp (accessed May 01, 2021).

[5] Chemisana D. Building integrated concentrating photovoltaics: A review. Renew Sustain Energy Rev 2011;15(1):603–11. https://doi.org/10.1016/j.rser.2010.07.017.

[6] Chow TT. A review on photovoltaic/thermal hybrid solar technology. Appl Energy 2010;87(2):365–79. https://doi.org/10.1016/j.apenergy.2009.06.037.

[7] Tyagi VV, Kaushik SC, Tyagi SK. Advancement in solar photovoltaic/thermal (PV/T) hybrid collector technology. Renew Sustain Energy Rev 2012;16(3):1383–98. https://doi.org/10.1016/j.rser.2011.12.013.

[8] Herrando M, Markides CN, Hellgardt K. A UK-based assessment of hybrid PV and solar-thermal systems for domestic heating and power: System performance. Appl Energy 2014;122:288–309. https://doi.org/10.1016/J.APENERGY.2014.01.061.

[9] Herrando M, Markides CN. Hybrid PV and solar-thermal systems for domestic heat and power provision in the UK: Techno-economic considerations. Appl Energy 2016;161:512–32. https://doi.org/10.1016/J.APENERGY.2015.09.025.

[10] Herrando M, Ramos A, Zabalza I. Cost competitiveness of a novel PVT-based solar combined heating and power system: Influence of economic parameters and financial incentives. Energy Convers Manag 2018;166:758–70. https://doi.org/10.1016/j.enconman.2018.04.005.

[11] Mellor A, Alonso Alvarez D, Guarracino I, Ramos A, Riverola Lacasta A, Ferre Llin L, et al. Roadmap for the next-generation of hybrid photovoltaic-thermal solar energy collectors. Sol Energy 2018;174:386–98. https://doi.org/10.1016/j.solener.2018.09.004.

[12] Yang CJ. Reconsidering solar grid parity. Energy Policy 2010;38(7):3270–3. https://doi.org/10.1016/j.enpol.2010.03.013.

[13] Ekins-Daukes NJ. Solar energy for heat and electricity: the potential for mitigating climate change. Grantham Inst Clim Chang Brief Pap 2009;1:1–12.

[14] Ju X, Xu C, Han X, Du X, Wei G, Yang Y. A review of the concentrated photovoltaic/thermal (CPVT) hybrid solar systems based on the spectral beam splitting technology. Appl Energy 2017;187:534–63. https://doi.org/10.1016/J.APENERGY.2016.11.087.

[15] Mojiri A, Taylor R, Thomsen E, Rosengarten G. Spectral beam splitting for efficient conversion of solar energy - A review. Renew Sustain Energy Rev 2013;28:654–63. https://doi.org/10.1016/j.rser.2013.08.026.

[16] Imenes AG, Mills DR. Spectral beam splitting technology for increased conversion efficiency in solar concentrating systems: a review. Sol Energy Mater Sol Cells 2004;84(1–4):19–69. https://doi.org/10.1016/J.SOLMAT.2004.01.038.

[17] S. S. Joshi, A. S. Dhoble, and P. R. Jiwanapurkar, "Investigations of Different Liquid Based Spectrum Beam Splitters for Combined Solar Photovoltaic Thermal Systems," *J. Sol. Energy Eng. Trans. ASME*, vol. 138, no. 2, 2016, doi: 10.1115/1.4032352.

[18] Widyolar B, Jiang L, Winston R. Spectral beam splitting in hybrid PV/T parabolic trough systems for power generation. Appl Energy 2018;209:236–50. https://doi.org/10.1016/J.APENERGY.2017.10.078.

[19] T. Otanicar, R. A. Taylor, P. E. Phelan, and R. Prasher, "Impact of size and scattering mode on the optimal solar absorbing nanofluid," in *Proceedings of the ASME 3rd International Conference on Energy Sustainability 2009, ES2009*, 2009, vol. 1, pp. 791–796, doi: 10.1115/ES2009-90066.

[20] Taylor RA, Otanicar T, Rosengarten G. Nanofluid-based optical filter optimization for PV/T systems. Light Sci Appl 2012;1:1–7. https://doi.org/10.1038/lsa.2012.34.

[21] Liang H, Han H, Wang F, Cheng Z, Lin B, Pan Y, et al. Experimental investigation of cost-effective ZnO nanofluid based spectral splitting CPV/T system. Energy 2020;194:116913. https://doi.org/10.1016/j.energy.2020.116913.

[22] Otanicar T, Dale J, Orosz M, Brekke N, DeJarnette D, Tunkara E, et al. Experimental evaluation of a prototype hybrid CPV/T system utilizing a nanoparticle fluid absorber at elevated temperatures. Appl Energy 2018;228:1531–9. https://doi.org/10.1016/j.apenergy.2018.07.055.

[23] Crisostomo F, Hjerrild N, Mesgari S, Li Q, Taylor RA. A hybrid PV/T collector using spectrally selective absorbing nanofluids. Appl Energy 2017;193:1–14. https://doi.org/10.1016/j.apenergy.2017.02.028.

[24] An W, Wu J, Zhu T, Zhu Q. Experimental investigation of a concentrating PV/T collector with Cu9S5 nanofluid spectral splitting filter. Appl Energy 2016;184:197–206. https://doi.org/10.1016/j.apenergy.2016.10.004.

[25] Liang H, Han H, Wang F, Cheng Z, Lin B, Pan Y, et al. Experimental investigation on spectral splitting of photovoltaic/thermal hybrid system with two-axis sun tracking based on SiO2/TiO2 interference thin film. Energy Convers Manag 2019;188:230–40. https://doi.org/10.1016/j.enconman.2019.03.060.

[26] Wang K, Pantaleo A, Herrando M, Faccia M, Pesmazoglou I, Franchetti BM, et al. Spectral-splitting hybrid PV-thermal (PVT) systems for combined heat and power provision to dairy farms. Renew Energy 2020;159:1047–65. https://doi.org/10.1016/j.renene.2020.05.120.

[27] Huang G, Wang K, Markides CN. Efficiency limits of concentrating spectral-splitting hybrid photovoltaic-thermal (PV-T) solar collectors and systems. Light Sci Appl 2021;10(1):2047–7538. https://doi.org/10.1038/s41377-021-00465-1.

[28] Wingert R, O'Hern H, Orosz M, Harikumar P, Roberts K, Otanicar T. Spectral beam splitting retrofit for hybrid PV/T using existing parabolic trough power plants for enhanced power output. Sol Energy 2020;202:1–9. https://doi.org/10.1016/j.solener.2020.03.066.

[29] Liew NJ, Yu ZJ, Holman Z, Lee HJ. Application of spectral beam splitting using Wavelength-Selective filters for Photovoltaic/Concentrated solar power hybrid plants. Appl Therm Eng 2022;vol. 201, no. PB:117823. https://doi.org/10.1016/j.applthermaleng.2021.117823.

[30] Huang G, Markides CN. Spectral-splitting hybrid PV-thermal (PV-T) solar collectors employing semi-transparent solar cells as optical filters. Energy Convers Manag 2021;248:114776. https://doi.org/10.1016/j.enconman.2021.114776.

[31] Wang Y, Song J, Chatzopoulou M, Sunny N, Simpson M, Wang J, et al. A holistic thermoeconomic assessment of small-scale, distributed solar organic Rankine cycle (ORC) systems: Comprehensive comparison of configurations, component and working fluid selection. Energy Convers Manag 2021;248:114618. https://doi.org/10.1016/j.enconman.2021.114618.

[32] J. Freeman, K. Hellgardt, and C. N. Markides, "An assessment of solar-powered organic Rankine cycle systems for combined heating and power in UK domestic applications," *Appl. Energy*, vol. 138, pp. 605–620, doi: 10.1016/J.APENERGY.2014.10.035.

[33] Freeman J, Hellgardt K, Markides CN. Working fluid selection and electrical performance optimisation of a domestic solar-ORC combined heat and power system for year-round operation in the UK. Appl Energy 2017;186:291–303. https://doi.org/10.1016/J.APENERGY.2016.04.041.

[34] Freeman J, Guarracino I, Kalogirou SA, Markides CN. A small-scale solar organic Rankine cycle combined heat and power system with integrated thermal energy storage. Appl Therm Eng 2017;127:1543–54. https://doi.org/10.1016/J.APPLTHERMALENG.2017.07.163.

[35] Al-Nimr MA, Bukhari M, Mansour M. A combined CPV/T and ORC solar power generation system integrated with geothermal cooling and electrolyser/fuel cell storage unit. Energy 2017;133:513–24. https://doi.org/10.1016/J.ENERGY.2017.05.142.

[36] K. Wang, A. M. Pantaleo, O. A. Oyewunmi, and C. N. Markides, "Flexible PVT-ORC hybrid solar-biomass cogeneration systems: the case study of the university sports centre in Bari, Italy," 2019. Accessed: Aug. 30, 2020. [Online]. Available: https://www.researchgate.net/publication/335776932.

[37] Kutlu C, Li J, Su Y, Wang Y, Pei G, Riffat S. Investigation of an innovative PV/T-ORC system using amorphous silicon cells and evacuated flat plate solar collectors. Energy 2020;203:117873. https://doi.org/10.1016/j.energy.2020.117873.

[38] "Therminol VP-1 Heat Transfer Fluid | Therminol | Eastman." https://www.therminol.com/product/71093459 (accessed Jul. 17, 2020).

[39] H. Jamali, "Investigation and review of mirrors reflectance in parabolic trough solar collectors (PTSCs)," *Energy Reports*, vol. 5. Elsevier Ltd, pp. 145–158, 01, 2019, doi: 10.1016/j.egyr.2019.01.006.

[40] "Dichroic Beamsplitters - Thorlabs." https://www.thorlabs.com/navigation.cfm?guide_id=2354 (accessed Mar. 07, 2021).
[41] Liu T, Lin W, Gao W, Luo C, Li M, Zheng Q, et al. A Parametric Study on the Thermal Performance of a Solar Air Collector with a V-Groove Absorber. Int J Green Energy 2007;4(6):601–22. https://doi.org/10.1080/15435070701665370.
[42] Lämmle M, Kroyer T, Fortuin S, Wiese M, Hermann M. Development and modelling of highly-efficient PVT collectors with low-emissivity coatings. Sol Energy 2016;130:161–73. https://doi.org/10.1016/j.solener.2016.02.007.
[43] Ma L, Lu Z, Zhang J, Liang R. Thermal performance analysis of the glass evacuated tube solar collector with U-tube. Build Environ 2010;45(9):1959–67. https://doi.org/10.1016/j.buildenv.2010.01.015.
[44] Toffolo A, Lazzaretto A, Manente G, Paci M. A multi-criteria approach for the optimal selection of working fluid and design parameters in Organic Rankine Cycle systems. Appl Energy 2014;121:219–32. https://doi.org/10.1016/j.apenergy.2014.01.089.
[45] Rayegan R, Tao YX. A procedure to select working fluids for Solar Organic Rankine Cycles (ORCs). Renew Energy 2011;36(2):659–70. https://doi.org/10.1016/j.renene.2010.07.010.
[46] Bao J, Zhao L. A review of working fluid and expander selections for organic Rankine cycle. Renew Sustain Energy Rev 2013;24:325–42. https://doi.org/10.1016/J.RSER.2013.03.040.
[47] Bhattarai S, Oh JH, Euh SH, Krishna Kafle G, Hyun Kim D. Simulation and model validation of sheet and tube type photovoltaic thermal solar system and conventional solar collecting system in transient states. Sol Energy Mater Sol Cells 2012;103:184–93. https://doi.org/10.1016/j.solmat.2012.04.017.
[48] "Photovoltaic Geographical Information System (PVGIS) | EU Science Hub." https://ec.europa.eu/jrc/en/pvgis (accessed Jul. 20, 2020).
[49] "Seville climate: Average Temperature, weather by month, Seville weather averages - Climate-Data.org." https://en.climate-data.org/europe/spain/andalusia/seville-2933/ (accessed Jul. 20, 2020).
[50] "Energy costs in Spain - Expat Guide to Spain | Expatica." https://www.expatica.com/es/living/household/energy-costs-108518/ (accessed Jul. 20, 2020).
[51] (accessed Jul 2017;20:2020). https://www.odyssee-mure.eu/publications/efficiency-by-sector/households/electricity-consumption-dwelling.html.
[52] "UK climate averages - Met Office." https://www.metoffice.gov.uk/research/climate/maps-and-data/uk-climate-averages (accessed Jul. 20, 2020).
[53] "Compare Gas and Electricity Prices per kWh | UKPower." https://www.ukpower.co.uk/home_energy/tariffs-per-unit-kwh (accessed Jul. 20, 2020).
[54] "Energy consumption in the UK - GOV.UK." https://www.gov.uk/government/statistics/energy-consumption-in-the-uk (accessed Jul. 20, 2020).
[55] "Muscat climate: Average Temperature, weather by month, Muscat water temperature - Climate-Data.org." https://en.climate-data.org/asia/oman/muscat/muscat-2089/ (accessed Jul. 20, 2020).
[56] "Oman electricity prices, December 2019 | GlobalPetrolPrices.com." https://www.globalpetrolprices.com/Oman/electricity_prices/ (accessed Jul. 20, 2020).
[57] Sweetnam T, Al-Ghaithi H, Almaskari B, Calder C, Gabris J, Patterson M. "Residential Energy Use In Oman. A Scoping Study Project Report" 2014.
[58] "PV Performance Modeling Collaborative | Spectral Response." https://pvpmc.sandia.gov/modeling-steps/2-dc-module-iv/effective-irradiance/spectral-response/?fbclid=IwAR3Es6t04nOdgdv6hJk2BJjviO65xwVWF2qqVI3tvhGDuL2mKb5eVUhJufs (accessed Jul. 06, 2020).
[59] Knechtli RC, Loo RY, Kamath GS. High-Efficiency GaAs Solar Cells. IEEE Trans Electron Devices 1984;31(5):577–88. https://doi.org/10.1109/T-ED.1984.21572.
[60] T. Otanicar, I. Chowdhury, P. E. Phelan, and R. Prasher, "Parametric analysis of a coupled photovoltaic/thermal concentrating solar collector for electricity generation," *J. Appl. Phys.*, vol. 108, no. 11, 2010, doi: 10.1063/1.3514590.
[61] Ni J, Li J, An W, Zhu T. Performance analysis of nanofluid-based spectral splitting PV/T system in combined heating and power application. Appl Therm Eng 2018;129:1160–70. https://doi.org/10.1016/j.applthermaleng.2017.10.119.
[62] Singh P, Ravindra NM. Temperature dependence of solar cell performance - An analysis. Sol Energy Mater Sol Cells 2012;101:36–45. https://doi.org/10.1016/j.solmat.2012.02.019.
[63] Notton G, Cristofari C, Mattei M, Poggi P. Modelling of a double-glass photovoltaic module using finite differences. Appl Therm Eng 2005;25(17–18):2854–77. https://doi.org/10.1016/j.applthermaleng.2005.02.008.
[64] Eastman, "Therminol VP-1 heat transfer fluid properties." https://www.therminol.com/sites/therminol/files/documents/TF09A_Therminol_VP1.pdf (accessed Mar. 27, 2021).
[65] J. A. Duffie, W. A. Beckman, and J. McGowan, *Solar Engineering of Thermal Processes* , vol. 53, no. 4. 1985.
[66] Hines AL, Maddox RN. Mass Transfer: Fundamentals And Applications 1985.
[67] Sieder EN, Tate GE. Heat Transfer and Pressure Drop of Liquids in Tubes. Ind Eng Chem Dec. 1936;28(12):1429–35. https://doi.org/10.1021/ie50324a027.
[68] Song J, Loo P, Teo J, Markides CN. Thermo-economic optimization of organic Rankine cycle (ORC) systems for geothermal power generation: A comparative study of system configurations. Front Energy Res 2020;8:1–14. https://doi.org/10.3389/fenrg.2020.00006.
[69] "HSE - Legionnaires' disease - Hot and cold water systems - Things to consider." https://www.hse.gov.uk/legionnaires/things-to-consider.htm (accessed Jul. 07, 2020).
[70] International Energy Agency, "Gas Fired Power," 2010. https://iea-etsap.org/E-TechDS/PDF/E02-gas_fired_power-GS-AD-gct_FINAL.pdf (accessed Jul. 10, 2020).
[71] Tocci L, Pal T, Pesmazoglou I, Franchetti B. Small Scale Organic Rankine Cycle (ORC): A Techno-Economic Review. Energies 2017;10(4):413. https://doi.org/10.3390/en10040413.
[72] Langdon LD. "Spon's Mechanical and Electrical Services Price" 2010.
[73] "Copeland ZR28K3E PFJ 522 scroll compressor | Wolseley." https://www.wolseley.co.uk/product/copeland-zr-28k3e-pfj-522-scroll-compressor————————cb/ (accessed Jul. 09, 2020).
[74] "Battery Pack Prices Fall As Market Ramps Up With Market Average At $156/kWh In 2019 | BloombergNEF." https://about.bnef.com/blog/battery-pack-prices-fall-as-market-ramps-up-with-market-average-at-156-kwh-in-2019/ (accessed Jul. 09, 2020).
[75] S. Quoilin Liège, "Sustainable Energy Conversion Through the Use of Organic Rankine Cycles for Waste Heat Recovery and Solar Applications," 2011.
[76] "Grundfos UPS3 15-50/65 130 circulating pump 1 x 230V 50Hz 9H GB | Wolseley." https://www.wolseley.co.uk/product/grundfos-ups3-15-50-65-130-circulating-pump-1-x-230v-50hz-9h-gb/ (accessed Jul. 09, 2020).
[77] seair, "Therminol VP-1 Import Data of India and Price," 2016. https://www.seair.co.in/therminol-vp1-import-data.aspx (accessed Jul. 09, 2020).
[78] "Domestic Oil Tanks | Bunded Oil Tanks | PlumbNation." https://www.plumbnation.co.uk/oil-tanks/ (accessed Jul. 09, 2020).
[79] I. Guarracino, J. Freeman, N. Ekins-Daukes, and C. N. Markides, "Performance assessment and comparison of solar ORC and hybrid PVT systems for the combined distributed generation of domestic heat and power," *Int. Conf. Heat Transf. Fluid Mech. Thermodyn.*, 2016, [Online]. Available: https://spiral.imperial.ac.uk/bitstream/10044/1/32640/2/Guarracinoetal_HEFAT2016.pdf.
[80] P. Kurup and C. S. Turchi, "Parabolic Trough Collector Cost Update for the System Advisor Model (SAM)," 2015. Accessed: Jul. 09, 2020. [Online]. Available: www.nrel.gov/publications.
[81] International Energy Agency, "Projected Costs of Generating Electricity 2015 – Analysis - IEA." https://www.iea.org/reports/projected-costs-of-generating-electricity-2015 (accessed Jul. 10, 2020).
[82] "Historic inflation – overview of CPI inflation year pages." https://www.inflation.eu/inflation-rates/historic-cpi-inflation.aspx (accessed Jul. 10, 2020).
[87] "What is the Return on Solar Panel Use in the UK? | GreenMatch." https://www.greenmatch.co.uk/blog/2014/07/how-long-will-a-solar-panel-take-to-pay-for-itself-in-the-north-of-uk (accessed Dec. 03, 2020).
[88] Department for Business Energy & Industrial Strategy, "Electrcity Generation Costs 2020," 2020. [Online]. Available: https://assets.publishing.service.gov.uk/government/uploads/system/uploads/attachment_data/file/911817/electricity-generation-cost-report-2020.pdf.
[89] Comittee on Climate Change, "Next Steps for UK Heat Policy - Annex 2: Heat in UK Buildings Today," 2016. [Online]. Available: https://www.theccc.org.uk/publication/next-steps-for-uk-heat-policy/.
[90] National Grid ESO, "Historic Generation Mix & Carbon Intensity," 2021. https://data.nationalgrideso.com/carbon-intensity1/historic-generation-mix (accessed Jan. 23, 2022).
[91] Parlimentary Office of Science & Technology, "Carbon Foorprint of Heat Generation," 2016. [Online]. Available: https://researchbriefings.files.parliament.uk/documents/POST-PN-0523/POST-PN-0523.pdf.